Pathogen-encoded evasion of CXCL10 and T cell responses

Alejandro L. Antonia[1], Monica I. Alvarez[1], Esme Trahair[1], Kyle D. Gibbs[1], Kelly J. Pittman[1], Alyson B. Barnes[1], Jeffrey S. Smith[2], Sudarshan Rajagopal[2,3], J. Will Thompson[4], R. Lee Reinhardt[5,6], Dennis C. Ko[1,7,8]

Affiliations

[1]Department of Molecular Genetics and Microbiology, School of Medicine, Duke University, Durham, NC 27710

[2]Department of Biochemistry, School of Medicine, Duke University, Durham, NC 27710

[3]Division of Cardiology, Department of Medicine, School of Medicine, Duke University, Durham, NC 27710

[4]Proteomics and Metabolomics Shared Resource, Center for Genomics & Computational Biology, School of Medicine, Duke University, Durham, NC 27710

[5]Department of Biomedical Research, National Jewish Health, Denver, CO 27710

[6]Department of Immunology and Microbiology, University of Colorado Anschutz Medical Campus, Aurora, CO 80045

[7]Division of Infectious Diseases, Department of Medicine, School of Medicine, Duke University, Durham, NC 27710

[8]Lead contact

*To whom correspondence should be addressed: Dennis C. Ko, 0048B CARL Building Box 3053, 213 Research Drive, Durham, NC 27710. 919-684-5834. dennis.ko@duke.edu. @denniskoHiHOST

Abstract

Clearance of intracellular pathogens, such as *Leishmania* (*L.*) *major*, depends on a well-regulated adaptive T cell response. Here we describe a pathogen-encoded mechanism to alter T cell recruitment by suppressing CXCL10, a chemokine that recruits CD4+ and CD8+ T cells by signaling through the CXCR3 receptor. *L. major* suppresses CXCL10 through the virulence factor and protease, glycoprotein-63 (*gp63)*. GP63 cleaves CXCL10 after amino acid A81, impairing T-cell chemotaxis *in vitro*. GP63 from either extracellular promastigotes or intracellular amastigotes is capable of cleaving CXCL10. Consistent with CXCL10 cleavage during infection, we observed GP63-mediated impairment of activated CD8+ T-cells in the draining lymph nodes of C57BL/6J^{WT} mice. Correspondingly, in C57BL/6J^{WT} mice, *gp63* deletion resulted in slower lesion development and a smaller maximum lesion size. However, infection in C57BL/6J$^{cxcr3-/-}$ mice revealed the delay to lesion development required CXCR3 signaling. Finally, *Salmonella enterica* and *Chlamydia trachomatis* infection also suppress CXCL10*,* demonstrating convergent evolution of this immune evasion strategy in diverse intracellular pathogens*.* Understanding mechanisms of CXCL10 evasion may facilitate the development of novel therapeutic strategies to treat intracellular pathogens.

Keywords: CXCL10; IP-10; leishmaniasis; Leishmania; gp63; leishmanolysin; T cell; CXCR3; Chlamydia; Salmonella

Author Summary

Leishmaniasis is an infectious disease that affects over one million people annually. It is caused by intracellular parasites that have evolved to evade the host's attempts to eliminate the parasite. The most common form of disease, cutaneous leishmaniasis, causes disfiguring skin lesions if the host immune system does not appropriately respond to the infection. A family of molecules called chemokines are critical for the recruitment of specific subsets of immune cells required to eliminate infection. Here, we demonstrate a novel mechanism that the parasite *Leishmania (L.) major* employs to disrupt the immune response by interfering with chemokine signaling. By this strategy, *L. major* uses a protease to cleave chemokines known to recruit T-cells required for fighting off infection. We show that *L. major* cleavage of these immune signals changes the recruitment of CD8+ T-cells and alters disease progression in mice. Finally, we observe that multiple common human intracellular pathogens, including *Chlamydia trachomatis* and *Salmonella enterica,* interfere with the same chemokines, suggesting a strong selective pressure to avoid this component of the immune response. Our study provides new insights into how intracellular pathogens interact with the host immune response to enhance pathogen survival and exacerbate disease outcomes.

Introduction

The ability to recruit and differentiate T cell populations is of paramount importance to providing pathogen protection through adaptive immunity. Parasites in the genus *Leishmania,* the etiologic agent for leishmaniasis, serve as a paradigm for studying T cell polarization in response to intracellular pathogens [1]. However, persistent gaps in the understanding of host and pathogen factors that influence T cell polarization and immune

cell recruitment contribute to the dearth of immunotherapeutics and vaccines. With no available vaccine and limited treatment options, *Leishmania* spp. continue to cause 1.2 million cases of cutaneous leishmaniasis (CL) and 0.4 million cases of visceral leishmaniasis annually (VL) [2]. A better understanding of host immunity and pathogen evasion strategies is imperative to develop alternative approaches to current therapies, which are limited by variable efficacy, high cost, and growing drug resistance [3].

T-helper (T_h) cell polarization has provided a framework to characterize the coordination of immune cell subsets required for the host to heal a cutaneous leishmaniasis infection [4]. Classes of CD4+ T_h cells are defined by the type of immune response they elicit and corresponding cytokine production. T_h1 cells, defined by the secretion of IFNγ, mediate a pro-inflammatory response effective at eliminating intracellular parasites. By contrast, T_h2 cells, defined by secretion of IL4, IL5, and IL13, promote immunity targeting large, extracellular parasites. When infected with *Leishmania* (*L.*) *major*, T_h2 responding mice develop non-healing lesions, whereas T_h1 responding mice clear the parasite and heal the lesion [5-7]. Corresponding work in humans shows that non-healing cutaneous lesions are characterized by T_h2 associated cytokines, and individuals resistant to lesion development have a higher predominance of T_h1 associated cytokines [8-11]. Subsequent work has focused on elucidating how these disparate cytokine responses recruit a broader set of immune cells that contribute to the type-1 immunity required for clearance of *Leishmania* spp. and other intracellular pathogens.

CD8+ cells contribute to intracellular pathogen clearance both indirectly through production of IFNγ and directly through production of cytolytic molecules such as perforin and granzyme. Although the nuances of what conditions make CD8+ T cells protective or

pathologic during *Leishmania* spp. infection specifically remain to be elucidated, CD8+ T cells have been implicated in productive immunity to both primary and secondary infection [12]. As part of the broader type-1 immune response against *L. major* infection, CD8+ cells are expanded in response to infection [13]. During primary infection, IFNγ production by CD8+ T-cells reinforces the development of a protective T_h1 response [14, 15]. Similar production of IFNγ by CD8+ T-cells has been observed to contribute to resistance to reinfection with *L. major* [16, 17]. In contrast, the role of cytotoxic effects of CD8+ T cells in the context of leishmaniasis is less clear. CD8+ cytotoxicity by perforin and granzyme has been observed in response to multiple *Leishmania* spp.; however, this function has variously been reported to protect against or exacerbate disease [18, 19]. The observation that a single cell type can both allow pathogen-mediated pathology by too little activity and host-mediated pathology by excess activity highlights the critical role of cytokine and chemokine signaling and dosage in regulating localization and activity of the immune response during infection.

One of the chemokines that specifically regulates localization of activity of CD8+ T-cells is CXCL10, or IFNγ Inducible Protein 10 (IP10). CXCL10 is part of a family of highly homologous chemokines, including CXCL9 and CXCL11, which bind to and activate the CXCR3 chemokine receptor (reviewed in [20]). These chemokines are primarily produced by monocytic cells in response to pathogens and participate in coordinating an IFNγ-dominated type-1 immune response. CXCR3 is primarily expressed on $CD8^+$ cytotoxic T lymphocytes and $CD4^+$ T_h1 cells, and to a lesser extent on NK cells, monocytes, and macrophages [13, 20-24]. In response to *Leishmania* spp., CXCL10 mRNA transcript is upregulated *in vitro* and *in vivo* [25-27]. CXCR3 reporter mice show

an increase in CD4+, CD8+, and NK+ cells expressing CXCR3 after *L. major, Salmonella enterica* serovar Typhimurium, and *Histoplasma capsulatum* infection [13]. Additionally, BALB/c mice, which traditionally are unable to control *Leishmania* spp. infection, demonstrate a defect in CXCR3 upregulation [28, 29]. Finally, exogenous CXCL10 is protective against both cutaneous and visceral leishmaniasis [30-33]. Thus, in coordinating a healing, adaptive type-1 immune response to intracellular pathogens, the host upregulates transcription of CXCL10 and its receptor to orchestrate recruitment of CXCR3+ CD8+ and CD4+ T cells.

Here, we report that *L. major* suppresses CXCL10 at the protein level to skew host T cell responses. This suppression occurs through the proteolytic activity of the virulence factor glycoprotein-63 (GP63) and abrogates CXCR3-dependent T cell migration. Correspondingly in C57BL/6J mice, the presence of GP63 impaired recruitment of CD8+ T-cells to the draining lymph nodes and delayed lesion formation. Finally, we observed CXCL10 suppression with other intracellular pathogens, including *Salmonella enterica* and *Chlamydia trachomatis,* demonstrating that diverse intracellular pathogens have developed convergent mechanisms to suppress CXCL10.

Results

L. major glycoprotein *63 (gp63)* suppresses CXCL10

To broadly screen for *L. major* manipulation of host immunity, we measured secreted levels of 41 cytokines following infection of lymphoblastoid cell lines (LCLs) with *L. major.* LCLs constitutively produce CXCL10, and incubation with *L. major* reduced CXCL10 levels by greater than 90% (Fig. 1A). We confirmed this result in LPS-stimulated

human THP-1 monocytes infected with *L. major* (Fig. 1B). We determined that *L. major* CXCL10 suppression is post-transcriptional. THP-1s exposed to *L. major* had 2.5-fold higher *CXCL10* mRNA relative to uninfected, despite the reduction in protein concentration found in culture supernatants (Fig. 1B). To test whether an *L. major*-secreted factor is responsible for CXCL10 suppression, we treated recombinant human CXCL10 with cell-free conditioned media obtained from cultured *L. major* promastigotes. Again, CXCL10 was reduced by 90% with the conditioned media (Fig. 1C). Together, these results were consistent with proteolytic degradation by a pathogen-secreted protease.

We hypothesized that CXCL10 suppression was mediated by glycoprotein-63 (GP63), a zinc-metalloprotease conserved among the *Trypanasoma* family of parasites and expressed in both the extracellular promastigote and intracellular amastigote life stages [34-37]. To test if GP63 is required to suppress CXCL10, we used a known GP63 inhibitor, the zinc-chelator 1,10-phenanthroloine [38]. 1,10-phenanthroline inhibited CXCL10-suppressive activity in *L. major* conditioned media (Fig. 1C). Consistent with GP63-mediated degradation of CXCL10, conditioned media from a promastigote culture of *L. major* deficient for *gp63* (Δ*gp63*) did not suppress CXCL10, whereas complementation with a single copy of *gp63* (*L. major* Δ*gp63*+1) restored CXCL10 suppression (Fig. 1D). Furthermore, heterologously expressed GP63 secreted from mammalian HEK293T cells was sufficient for complete CXCL10 suppression, while a single point mutation in the catalytic site of GP63 (E265A) abrogated suppression (Fig. 1E). Therefore, GP63 is both necessary and sufficient for CXCL10 suppression by *L. major.*

GP63 cleaves the CXCL10-related family of chemokines

As GP63 has a diverse set of identified *in vitro* substrates [35], we examined the specificity of GP63 across a spectrum of chemokines. Based on the initial cytokine screen (Figure 1A), we hypothesized GP63 cleavage would be restricted to CXCL10 and highly related chemokines. To experimentally test for GP63 cleavage, purified recombinant chemokines were incubated with conditioned media from *L. major* WT, *L. major* Δ*gp63,* or *L. major* Δ*gp63+1.* GP63 cleavage was observed for CXCL9 (38.14% amino acid identity with CXCL10) and CXCL11 (30.85% amino acid identity with CXCL10) (Figure 2A, B), which both signal through CXCR3. By contrast, no cleavage of CXCL8 (IL-8; a neutrophil-attracting chemokine) or CCL22 (MDC; a Th2-attracting chemokine) was detected (Fig. 2B). Thus, chemokine cleavage by GP63 appears to preferentially degrade chemokines involved in CXCR3 signaling.

Although western blot analysis supported GP63-dependent cleavage through loss of CXCL10 immunoreactivity, it could not reveal the cleavage site. The GP63 consensus cleavage site has been described as polar, hydrophobic, and basic amino acids at positions P1, P1', and P2' [39]. Following this pattern, there are three potential cleavage sites in the mature CXCL10 protein (from amino acid position 22-96) that are conserved between human and murine CXCL10 (68.37% amino acid identity) (Fig. 2A). In order to characterize the cleavage product(s), we incubated GP63 with human recombinant CXCL10 and visualized a shift in size by total protein stain (Fig. 2C). Intact CXCL10 and the largest cleavage products were determined to be 8.8kD and 6.6kD respectively, by capillary electrophoresis-mass spectrometry (CE-MS) (Fig. 2D). After running the sample on a PAGE gel, the 8.8kD (intact, "Hi") product, 6.6kD (cleaved, "Lo") product, and an

uncleaved control ("Ctrl") were sequenced by trypsin digestion followed by liquid chromatography-tandem mass spectrometry (LC-MS/MS). Comparison of peptides after trypsin digest revealed a peptide from amino acids (AA) 74-81 that was exclusively present in the cleaved CXCL10 band, but notably absent in the uncleaved band (Fig. 2E). Conversely, distal peptide fragments such as AA84-91 were only present in the uncleaved CXCL10. This analysis demonstrated cleavage occurring in between A81 and I82, resulting in the loss of detectable peptides beyond those amino acids in cleaved CXCL10. This is consistent with the fragment size based on intact molecular weight CE-MS, and notably AIK (AA 81-83) is one of the three potential cleavage sites identified in our comparative analysis (see Figure 2A). To confirm this site as preferred for GP63 cleavage, we used site-direct mutagenesis to mutate the residues in the proposed cleavage motif. Mutation of the identified P1 residue significantly slowed CXCL10 cleavage in a time course experiment (Fig. 2F). Mapping the residues onto the crystal structure of CXCL10 [40] demonstrated that cleavage occurs at the beginning of the C-terminal alpha-helix of CXCL10 (Fig. 2G).

GP63 produced by *L. major* promastigotes or amastigotes can cleave CXCL10 protein

Immediately after injection by the sand-fly vector, *Leishmania* parasites exist as an extracellular, flagellated promastigote but are rapidly phagocytized where they transform into the intracellular, aflagellated amastigote parasite stage. We hypothesized that GP63 would continue to be able to suppress CXCL10 through both stages of infection, as transcriptomics indicate GP63 expression during both stages [37]. To test the capacity of *L. major* to suppress CXCL10 in both the promastigote and amastigote stage of infection,

we utilized PMA differentiated THP-1 monocytes as an intracellular macrophage model of infection. Differentiated THP-1 monocytes were infected at an MOI of 20 with promastigotes from *L. major WT, Δgp63,* or *Δgp63+1.* Extracellular promastigote activity was assessed in the supernatant at 24 hours post infection, followed by washing to remove the extracellular promastigotes and gp63 protein in the media and assess intracellular amastigote activity at 48 hours post infection.

This model demonstrated CXCL10 protein suppression by GP63 in both stages of the parasite life cycle. *L. major WT* promastigotes reduced CXCL10 protein below that produced by uninfected cells, while *L. major Δgp63* infection resulted in a significant induction of CXCL10 protein (Fig. 3A). Similarly, the *L. major WT* amastigotes continued to suppress CXCL10 protein significantly while *L. major Δgp63* infection significantly induced CXCL10 protein (Fig. 3B). The complementation observed with the *L. major Δgp63+1* strain is significant, though incomplete in the promastigote stage and further reduced in the amastigote stage. This is attributable to the plasmid construct being designed for high expression in the promastigote stage [41] and the lack of G418 selection during the experiment. Notably, all three *L. major* strains cause comparable induction of *CXCL10* mRNA (Fig. 3C). Together these results indicate that CXCL10 suppressing activity of GP63 is present in both parasite life cycle stages involved in infection in mammalian hosts.

GP63 alters recruitment of CD8+ T cells in the draining lymph node of infected mice

Because CXCL10 coordinates the recruitment of CXCR3+ T cells during infection, we next tested if GP63 cleavage of CXCL10 impacts T cell recruitment *in vitro* and *in vivo*. We tested the chemotactic ability of cleaved CXCL10 to recruit Jurkat T cells expressing

CXCR3. The basal chamber of a transwell system was seeded with CXCL10 in the presence of conditioned media from *L. major WT, L. major ∆gp63,* or *L. major ∆gp63+1.* Conditioned media from *L. major* WT and *L. major ∆gp63+1* abrogated CXCL10 induced migration of CXCR3+ Jurkat T cells, whereas the *L. major ∆gp63* conditioned media did not impair chemotaxis (Fig. 4A).

To determine if chemokine-mediated T cell recruitment is similarly impaired due to the activity of GP63 *in vivo,* we assessed T cell populations in the draining lymph node and at the site of the lesion in infected mice. We hypothesized that there would be a difference in CD8+ T cell recruitment, because CD8+ T cells highly express CXCR3 [20]. We assessed changes to the frequency and activation state of CD8+ T cells by flow cytometry and immunofluorescence staining in IFNγ reporter mice [42, 43]) (Fig. 4B). *L. major ∆gp63* infection resulted in a significant increase in the frequency of CD8+ T cells in the draining popliteal lymph nodes as assessed by flow cytometry relative to WT infection (Fig. 4C and E). At the site of the lesion, we assessed CD8+ T cell migration by immunofluorescence staining. Similar to observations in the draining lymph node, while not statistically significant, *L. major ∆gp63* infections had more CD8+ T cells at the site of the lesion compared to both the *L. major WT* and *L. major ∆gp63+1* infections (Fig. S1). These data are consistent with GP63 impairing chemotaxis of CD8+ T cells.

Additionally, we examined IFNγ and CD44 as markers of T cell activation (Fig. 4D). Secretion of IFNγ is one mechanism by which effector CD8+ T cells activate an anti-parasitic immune response [14, 15] while CD44 is a marker of activation or memory which co-expresses with CXCR3 [44]. The CD8+ T-cell populations in the draining lymph node of mice infected with *L. major ∆gp63* compared to *L. major WT* were enriched for CD44

expression (Fig. 4F; $p = 0.1$), Further, *L. major ⊿gp63* resulted in a significant increase in CD44+ cells among IFNγ+, CD8+ double positive cells (Fig. 4G; $p < 0.0001$). The lower proportion of CD44+ cells in *L. major* WT likely reflects reduced CXCR3 stimulation due to GP63 cleaving its ligands. Altogether, the differences in CD8+ T cell subsets between *L. major* WT and *⊿gp63* indicates that by evading CXCR3 stimulation, GP63 significantly alters the host T cell response.

CXCR3 ligands contribute to the delay in lesion development and healing phenotype caused by loss of *gp63*

Earlier studies of *L. major ⊿gp63 in vivo* identified its role as a virulence factor [45]. These studies were performed exclusively in the *L. major* susceptible BALB/c mouse genetic background and did not define the role for particular *gp63* substrates in pathogenesis. With evidence that GP63 disrupts T cell chemotaxis in C57BL/6J mice, we tested for a genetic interaction between gp63 and cxcr3. C57BL/6J mice mount a T_h1 and robust CD8+ T cell response while exhibiting a healing phenotype for infection with most *L. major* strains [1, 6]. Despite recruiting the appropriate subsets of T cells, C57BL/6J mice are paradoxically unable to clear infection with *L. major* Seidman, which was the parental strain used to make the *gp63* knockout [45, 46]. To investigate contributions of CXCR3 signaling to *gp63* phenotypes, we utilized wild-type (C57BL/6J^{WT}) and CXCR3 knockout (C57BL/6J$^{CXCR3-/-}$; Jackson Lab B6.129P2-*Cxcr3*^{tm1Dgen}/J, 005796) mice. Although C57BL/6J$^{CXCR3-/-}$ mice are unable to control *L. major* WT infection [47], the impact of *gp63* in the absence of CXCR3 has not been investigated. We hypothesized that *L. major* WT evades immunity and causes more severe disease than ***Δgp63*** in mice

with functional CXCR3 signaling but that this advantage would be reduced in the absence of CXCR3 signaling.

To quantify disease progression, we measured changes in footpad thickness in C57BL6/J^{WT} and C57BL/6J$^{CXCR3-/-}$ mice infected with either *L. major WT, Δgp63,* or, *Δgp63+1*. *L. major Δgp63* infection exhibited differences from WT and *Δgp63+1* in C57BL/6J^{WT} but not C57BL/6J$^{CXCR3-/-}$ mice (Fig. 5A-B). This is apparent by analyzing specifically the length of time required for lesions to start developing. On the C57BL/6J^{WT} background, *L. major Δgp63* had delayed lesion development relative to WT and *Δgp63*+1. However, this advantage for *gp63* was not observed to the same extent in the C57BL/6J$^{CXCR3-/-}$ mouse background (Fig. 5C). This effect depended upon the interaction between *gp63* and *Cxcr3* (2-way ANOVA interaction term, p=0.02) (Fig. 5C). Thus, the delay in lesion kinetics required CXCR3 signaling, which provides strong genetic evidence that CXCR3 ligands are important for the effect of GP63 during cutaneous leishmaniasis infection.

L. major Δgp63 also reduced maximum lesion size in C57BL6/J mice, but this was independent of host CXCR3 genotype (Fig. 5D). Both *L. major* WT and *Δgp63* produced bigger lesions in C57BL/6J$^{CXCR3-/-}$ than in C57BL/6J^{WT}, suggesting that the impact of CXCR3 on maximum lesion size is GP63-independent (Fig. 5D). This independence from CXCR3 signaling is consistent with GP63 also cleaving other, previously described substrates to contribute to its complex impact on pathogenesis [35].

The incomplete complementation phenotype, observed both in THP-1 cells (see Figure 3) and in mice (Figure 5), reflects limitations of the complementation plasmid used

to generate the *L. major Δgp63+1* strain. Plasmid complementation of *gp63* (*Δgp63+1;* [45]) demonstrated only partial restoration of phenotypes towards the WT strain. However, interpretation is complicated as only 1 out of the 7 deleted *gp63* copies are encoded on the plasmid, and the absence of G418 selection *in vivo* results in gradual loss of the plasmid (Fig. S2). As the construct was designed for optimal expression in the promastigote parasite stage which predominates during early stages of infection, it is possible that like amastigote culture (Fig. 3B) the effect size of *gp63+1* plasmid *in vivo* is reduced later in infection. Of note, the delay in lesion development and reduced maximum lesion size was consistent with studies conducted previously in BALB/c mice and replicated here ([45] and Fig. S3). Overall, we conclude that *gp63* increases virulence by accelerating the time to lesion development and increasing maximum lesion size in C57BL/6J mice infected with *L. major.* While the effect on time to lesion development is CXCR3-dependent, the effect on maximum lesion size is CXCR3 independent and may depend on other reported GP63 substrates (reviewed in [35]).

CXCL10 suppression has evolved independently in multiple intracellular pathogens

Given that type-1 immunity and CXCR3+ immune cells broadly promote clearance of intracellular pathogens, we asked if other intracellular pathogens also suppress CXCL10. CXCL10 production by LCLs was measured by ELISA after exposure to a variety of pathogens including *Toxoplasma* (*T.*) *gondii*, *Plasmodium* (*P.*) *bergei*, *Salmonella* (*S.*) *enterica*, *Chlamydia* (*C.*) *trachomatis*, *Mycobacterium* (*M.*) *marinum, Mycobacterium* (*M.*) *smegmatis*, *Staphylococcus* (*S.*) *aureus,* and *Cryptococcus* (*C.*) *neoformans.* CXCL10 suppression of at least 80% was observed with two additional

intracellular pathogens: *S. enterica* and *C. trachomatis.* In contrast, other pathogens, including the extracellular pathogens *S. aureus* and *C. neoformans,* exhibited modest to no suppression of CXCL10 (Fig. 6). Thus, multiple intracellular pathogens that pose significant health burdens around the globe have independently evolved the ability to suppress CXCL10.

Discussion

We describe a pathogen-encoded mechanism for influencing host T cell recruitment in response to intracellular pathogens. Specifically, the *L. major* protease GP63 cleaves CXCR3 ligands to bypass CXCR3 signaling, impair CD8+ T cell localization, and exacerbate disease progression. Our approach combining biochemistry, genetics, and animal modeling led to insights regarding *Leishmania* spp. virulence factors that manipulate the recruitment of immune cell subsets to the parasite's advantage, and broadly how intracellular pathogens manipulate the immune system to avoid an appropriate adaptive immune response.

Our discovery that an *L. major*-encoded protease cleaves CXCL10 revealed a strategy for evading immune cells that express CXCR3 in the draining lymph node and at the site of the lesion. These results are particularly interesting in light of several recent reports highlighting the importance of CXCL10 and CXCR3 for CD8+ response to pathogens broadly. Strikingly, our observed decrease in effector CD44+ CD8+ T cells when CXCR3 signaling is disrupted by GP63 in *L. major* WT infections (Fig. 4D) phenocopies the decrease in effector T cells observed upon CXCR3 deletion previously described [48]. Further, CXCL10 has been demonstrated to precisely coordinate effector

CD8+ T cells to the site of *Toxoplasma gondii*, another intracellular eukaryotic pathogen [49]. In response to *Leishmania* spp. specifically, multiple studies demonstrate that CXCR3 ligands are recruited during infection. Majumder et al. report that CXCL10 recruits an *L. donovani* specific set of CD8+ cells [50], and Oghumo et al. demonstrated that CD8+CXCR3+CD44+ T cells expand after infection and have different functions from CXCR3-CD8+ T cells [13]. Further, CXCR3 expression has been reported on a wide range of other cells including NK, NKT, innate lymphocytes, and certain subsets of dendritic cells, B cells, and endothelial cells [13, 20-24]. Expression of CXCR3 on these diverse cell types with roles in antimicrobial immunity highlights the importance of evading this signaling pathway for pathogens.

However, the precise impact these CD8+ cells have on disease outcomes in cutaneous leishmaniasis remains unclear. CD8+ T cells have two anti-leishmanial mechanisms: production of type-1 associated cytokines, particularly IFNγ, to promote CD4+ T_h1 differentiation and activate macrophage-stimulated parasite killing [14, 15], and cytotoxicity that directly kills infected cell with granzyme B and perforins [51, 52]. However, in both humans and mice, CD8+ cytotoxic effects have been associated with severe host-mediated pathology and parasite metastasis in certain contexts [12]. GP63 cleavage may therefore regulate parasite clearance and spread but also host-mediated pathology.

Current limitations of parasite genetics and the animal model of leishmaniasis may contribute to an incomplete picture of the impact of GP63 on chemokine signaling. First, sequencing *L. major* revealed proteins distantly homologous to GP63 (approximately 35% amino acid identity) on chromosomes 24 and 31, in addition to the tandem array of *gp63*

genes on chromosome 10 [34, 53]. These related proteases may suppress CXCL10 during different stages of infection, or cleave an additional set of host substrates even though they are not required for CXCL10 cleavage under our *in vitro* conditions. Second, *L. major ⊿gp63+1* has one of the seven chromosome-10 *gp63* copies maintained on a plasmid under G418 selection and optimized for expression in promastigotes [41]. Because of G418 toxicity in mice, we were unable to maintain chemical selection, and the relative copy number decreased at the end of infection (Fig. S3). Complementation with only one copy of GP63, loss of plasmid, and lower amastigote expression from the plasmid likely contribute to the incomplete complementation of infection phenotypes. Third, the CD8+ response to *Leishmania* spp. infection is greater with lower dose infections ($1x10^3$ promastigotes) [14, 15]. The infections in this study were performed using the high dose infection model ($2x10^6$ promastigotes), and therefore the effect of CXCR3 evasion may be greater under different infection conditions. Despite these limitations, we clearly describe an *in vivo* context during which GP63 disruption of CXCR3 signaling alters immune cell recruitment. Further investigation will be required to elucidate the implications of this novel mechanism of immune evasion in other infection contexts.

Our finding that GP63 mediates a parasite-encoded mechanism to evade a key signaling pathway for immune memory highlights the potential for a shift in design strategy of a *Leishmania* vaccine. An effective vaccine to protect against leishmaniasis has been a tantalizing strategy for disease control with unrealized potential. Historically, inoculation with live parasites in unexposed areas of skin has effectively prevented future infections [54]; however, this strategy poses significant risks, particularly with the increase of HIV co-infection [55-57], and is not an accepted medical practice. Despite the success of this

rudimentary form of vaccination and promising results in animal studies, vaccines have consistently failed to confer long term protection in human studies partly due to persistent gaps in understanding of the factors that confer immunity to leishmaniasis [54].

An emerging theme in the effort to better understand what confers long term immunity is the role of chemokine recruitment. Transcription of *Cxcl10* is significantly upregulated in response to secondary infection relative to primary infection, and antibody blockade of the CXCR3 receptor prevents recruitment of T resident-memory (T_{rm}) cells to the site of secondary infection [58-60]. In combination with these findings, the observation that CXCR3 substrates are cleaved *in vivo* by *Leishmania* spp. suggests that one of the goals of vaccine development should be to overcome parasite-encoded CXCR3 escape upon secondary infection. Promisingly, GP63-specific CD4+ T cells elicit strong IFNγ and T_h1 responses [61]. Strategies that use the GP63 protein as an antigen or adjuvant report long term immunity in mice that is correlated with T_h1 responses [62-65]; a phenotype that could be enhanced by anti-GP63 antibodies functionally blocking cleavage of CXCR3 ligands. A complete understanding of how the parasites alters chemokine recruitment upon secondary infection will be paramount to developing a vaccine that can provide long term immunity to leishmaniasis.

The relevance of these insights into immune evasion and vaccine design is made more impactful by the observation that CXCL10 suppression has arisen in multiple intracellular pathogens. We found that *L. major, S. enterica*, and *C. trachomatis* independently evolved mechanisms to suppress CXCL10, which indicates that suppression of CXCR3 inflammatory signaling is advantageous for multiple intracellular pathogens. In addition to *S. enterica* and *C. trachomatis,* several commensal and

pathogenic bacteria suppress CXCL10, including *Lactobacillus paracasei*, *Streptococcus pyogenes, Finegoldia magna*, and *Porphymonas gingivalis* [66-68]. Similarly, the fungal pathogen *Candida albicans* produces a signaling molecule to inhibit CXCL10 transcription [69]. Among viruses, Hepatitis C virus (HCV) upregulates host proteases to modify CXCL10 [70], Epstein-Barr virus (EBV) decreases transcription through chromatin remodeling at the *CXCL10* locus [71], and Zika virus (ZIKV) blocks translation of CXCL10 [72, 73]. The repeated and independent evolution of CXCL10 evasion suggests that this chemokine poses a significant evolutionary pressure on common human pathogens. These diverse pathogens heavily impact global morbidity and mortality. Understanding how pathogens manipulate the CXCR3 signaling axis to their advantage may enable therapeutic countermeasures that circumvent or prevent pathogen suppression of CXCR3 signaling.

Materials/Methods

Cell Lines

LCLs from the International HapMap Project [74] (GM18524 from Han Chinese in Beijing, China, GM19203 from Yoruba in Ibadan, Nigeria, and GM7357 from Utah residents with Northern and Western European ancestry from the CEPH collection) were purchased from the Coriell Institute. LCLs were maintained at 37˚C in a 5% CO2 atmosphere and were grown in RPMI 1640 media (Invitrogen) supplemented with 10% fetal bovine serum (FBS), 2 mM glutamine, 100 U/ml penicillin-G, and 100 mg/ml 790 streptomycin. THP-1 monocytes, originally from ATCC, were obtained from the Duke Cell Culture Facility and maintained in RPMI 1640 as described above. HEK293T cells were obtained from ATCC

434 and maintained in DMEM complete media (Invitrogen) supplemented with 10% FBS,
435 100U/ml penicillin-G, and 100mg/ml 790 streptomycin. Jurkat cells (an immortalized T cell
436 line) stably expressing CXCR3 were generated by transfecting a linearized pcDNA3.1
437 expression vector encoding *CXCR3* and resistance to Geneticin (G-418), selecting for
438 transfected cells with 1000 μg/mL Geneticin, and collecting highly expressing CXCR3
439 cells by FACS. Cells were maintained in RPMI 1640 media (Sigma) supplemented with
440 10% FBS, 1% Penicillin/Streptomycin, 0.23% Glucose, 10mM HEPES, 1mM Sodium
441 Pyruvate, and 250 µg/mL Geneticin.
442
443 *Mice*
444 IACUC approval was obtained through Duke University (protocol# A200-15-07). The
445 following mice were obtained from the Jackson Laboratory and maintained by the Duke
446 Division of Lab Animal Resources (DLAR) Breeding Core. C57BL/6J^{WT} (C57BL/6J,
447 000664), BALB/c^{WT} (BALB/cJ, 000651), C57BL/6J$^{cxcr3-/-}$ (B6.129P2-*Cxcr3*^{tm1Dgen}/J,
448 005796). The GREAT, IFNγ-reporter, mice were obtained from Dr. Richard
449 Reinhardt [42, 43]. As the CXCR3 allele is an X-linked trait, the C57BL/6J$^{cxcr3-/-}$ mice
450 were maintained by crossing heterozygous females (C57BL/6J$^{cxcr3+/-}$) with hemizygous
451 males (C57BL/6J$^{cxcr3-/y}$). For all infections, mice were matched by litter, sex, and age (6-
452 13 weeks at time of inoculation) prior to being randomly assigned to an infection group.
453 For *L. major* infections in C57BL/6J$^{cxcr3-/-}$, comparisons were made between knockout
454 (litter-matched male C57BL/6J$^{CXCR3-/y}$ and female C57BL/6J$^{CXCR3-/-}$) to wildtype (litter-
455 matched male C57BL/6J$^{cxcr3+/y}$, and non-litter matched female C57BL/6J$^{cxcr3+/+}$, as this
456 genotype cannot be generated by our mating strategy).

Pathogen culture and infections.

Leishmania spp. were obtained from BEI (*L. major WT* ((MHOM/SN/74/Seidman), NR-48819), *L. major Δgp63* ((MHOM/SN/74/SD) *Δgp63 1-7,* NR-42489), *L. major Δgp63+1* (MHOM/SN/74/SD) *Δgp63 1-7* + *gp63-1,* NR-42490)). Parasites were maintained at 27°C in M199 media (Sigma-Aldrich, M1963), supplemented with 100u/ml penicillin/streptomycin, and 0.05% Hemin (Sigma-Aldrich, 51280). Cultures were split 1:20 every 5 days into 10mL of fresh culture media. To prepare parasites for infection, 8mL of a 5-day-old culture was spun at 1200g for 10 min and washed with 5mL of HBSS prior to counting promastigotes with a hemocytometer and resuspending at the indicated concentration. As relevant controls in using these *L. major* strains, we replicated the previously reported lesion progression phenotypes [45] using WT, *Δgp63*, and *Δgp63+1* strains in BALB/c mice (Fig. S2A) and found the strains contained similar levels of metacyclic parasites based on flow cytometric measurement and metacyclic enrichment with peanut agglutinin (Fig. S2B).

For infections of LCLs and THP-1 monocytes, $1x10^5$ cells were placed in 100μl of RPMI 1640 assay media as described above, with no penicillin/streptomycin added. In the case of THP-1 monocytes, cells were then stimulated with 1μg/mL of LPS derived from *Salmonella enterica* serovar typhimurium (Enzo Bioscience, ALX-581-011-L001). Finally, $1x10^6$ *L. major* promastigotes were added in 50μL of RPMI 1640 assay media for a multiplicity of infection (MOI) of 10. Culture supernatants and cell pellets were collected after 24 hours of infection. For phorbol 12-myristate 13-acetate (PMA) differentiation of THP-1 monocytes, $1.2x10^6$ cells were placed in 2mL of complete RPMI 1640 media

supplemented with 100ng/mL of PMA for 8 hours after which the RPMI media was replaced and cells allowed to rest for 36 hours. Parasites were then washed and counted as described above and added at an MOI of 20. At 24 hours post-infection, the culture supernatant was removed, spun at 1200g for 10 minutes to separate extracellular parasites, and stored at -20C for downstream cytokine analysis. Cells were then washed 3 times with 1mL of PBS followed by one additional wash with 2mL of RPMI media to remove the remaining extracellular promastigotes. At 48 hours post infection the culture supernatant was collected and stored for downstream analysis. All cells were stored in 1mL of RNAprotect (Qiagen, 76526) at -20C for downstream RNA extraction (RNeasy Mini Kit, Qiagen, 74106) and qPCR analysis.

For murine infections, parasites were resuspended in HBSS at a concentration of $2x10^6$ total promastigotes in 50µl of HBSS. We confirmed that the inoculums from *L. major* WT*, L. major ∆gp63,* and *L. major ∆gp63+1* had comparable rates of infectious metacyclic promastigotes by analyzing a frozen aliquot of parasites from the same batch used for all mouse experiments in this study with a combination of PNA selection and flow cytometric analysis (Fig. S2) [75, 76]. Mice were anesthetized using isofluorane prior to subcutaneous inoculation of 50µl parasite preparation into left hind footpad with a 27 gauge tuberculin syringe (BD Biosciences, 305620). Lesion progression was monitored every five days by measuring footpad thickness using a thickness gauge (Mitutoyo, catalogue # 7301). Mice were considered to reach a humane endpoint prior to the end of the study if ulceration of the lesion was observed. Early removal of a mouse from the experiment due to humane endpoint is indicated in the corresponding figure legend. DNA was used to measure parasite burden as described previously [77]. In brief, DNA was

harvested from infected tissue using the DNeasy Blood and Tissue kit (Qiagen). DNA was amplified by RT-PCR for the *L. major* DRBD4 gene, and each sample quantified relative to a standard curve of known parasite DNA.

Infections with *Salmonella enterica* serovar Typhimurium*, Chlamydia trachomatis,* and *Toxoplasma gondii* (RH and Prugniaud A7) were performed as described previously [78]. For *Staphylococcus aureus,* LCLs were plated at 40,000 cells per 100μl RPMI assay media in 96-well plates prior to inoculation at an MOI of 10 with *S. aureus* Sanger-476. Cells were spun at 200xg for 5 minutes prior to incubation at 37°C for 1 hour. Gentamicin was added at 50μg/ml and then supernatant was collected at 24 hours. For *Cryptococcus neoformans,* LCLs were plated at 40,000 cells per 100μl RPMI assay media in 96-well plates prior to inoculation at an MOI of 5 with *C. neoformans* H99 strain. Cells were incubated at 37°C for 24 hours prior to collection of supernatant. For *Plasmodium berghei* infections, LCLs were plated at 40,000 cells per 100μl RPMI assay media in 96-well plates prior to inoculation with 17,000 *P. berghei*-Luciferase sporozoites isolated from *Anopheles stephensi* from the New York University Insectary Core Facility. Cells were spun at 1000xg for 10 minutes prior to incubation at 37ºC for 48 hours. Cell death was monitored by 7AAD staining and quantified using a Guava easyCyte HT flow cytometer. To harvest supernatants, LCLs were centrifuged at 200xg for 5 minutes prior to removing supernatant and storing at -80ºC prior to quantifying chemokines production by ELISA. For *Mycobacterium marinum* and *Mycobacterium smegmatis* infections, LCLs were plated at 40,000 cells per 100μl RPMI assay media without FBS and supplemented with 0.03% bovine serum albumin (BSA) prior to infection with 400,000 bacteria per well. Cells were spun at 100xg for 5 minutes prior to incubation at 33ºC for 3 hours, after which 50μl

of streptomycin in RPMI media was added for a final concentration of 200μg/ml streptomycin with 10% FBS, and incubation was continued at 33ºC for 24 hours. Cell death was monitored by 7AAD staining and quantified using a Guava easyCyte HT flow cytometer. To harvest supernatants, LCLs were centrifuged at 200xg for 5 minutes prior to removing supernatant and storing at -80ºC prior to quantifying chemokines by ELISA.

In vitro *T cell migration*

RPMI 1640 media (Sigma) was supplemented with 2% FBS and CXCL10 at a starting concentration of 100nM. This was pre-incubated at a ratio of 1:1 with conditioned media from either *L. major WT, Δgp63,* or *Δgp63+1*. After 12 hours of pre-incubation, 600µl of CXCL10/conditioned media mix was added to a 24 well plate. 500,000 Jurkat T cells stably transfected with *CXCR3* were seeded onto the apical membrane of the 5μm transwell insert (Corning, 3421), and allowed to incubate at 37°C for 4 hours. The transwell insert was removed and the concentration of cells in the basal chamber determined using a Guava easyCyte HT flow cytometer (Millipore).

Flow cytometry

Draining, popliteal lymph nodes were harvested from GREAT mice at 59 days post infection and immediately placed into RPMI complete media supplemented with 10% HI-FBS and stored on ice. Lymph nodes were mechanically dissociated, passed through a 70µm cell strainer (Corning, 431751), and washed with 10mL of sterile PBS. Cells were then spun at 300xg for 5 minutes, resuspended in FACS buffer (Sterile PBS supplemented with 2% heat inactivated FBS), and counted using Guava Easycyte Flow

Cytometer prior to staining. For staining, the following antibodies were used: B220 (PE-Cy7, Thermo 25-0452-82), CD3 (APC-Cy7, 100222), CD8 (PE-Cy5, Biolegend 100710), CD4 (BV605, Biolegend 100451), and CD44 (PE, Biolegend 103007). Cells were analyzed using a BD LSRII flow cytometer at the Duke Human Vaccine Institute (DHVI) Flow Cytometry Shared Resource. For each set of infections, HBSS mock infected mice were included on which negative gates were set. FlowJo (version 10.3) was used to gate on live (DAPI negative), singlet cells in the lymphocyte gate (based on FSC v SSC). Subsequently, samples gated as B220-negative were stratified by CD4+ and CD8+ staining. Within each, CD4+ or CD8+ cells were then gated based on the IFNγ-YFP reporter and CD44 as markers of T cell polarization and activation.

Immunofluorescence staining

Infected mouse footpads were harvested and immediately placed in 1mL of 4% paraformaldehyde (PFA) and allowed to incubate at 4°C on a rocker overnight. Samples were then washed with 1mL of PBS and returned to 4°C for 8 hours. Subsequently, they were placed in a 30% sucrose solution and incubated at 4°C overnight, after which they were placed in OCT, flash frozen in liquid nitrogen, and stored at -80°C. Samples were sectioned into 10μm sections using a cryostat (Leica, CM1950). For each tissue, 6 tissue sections were placed on each of 3 separate slides. Each slide was separated by at least 100μm from the others to represent the full extent of the site of infection.

For tissue staining, slides were covered with blocking buffer (PBS, 0.5% normal donkey serum, and 0.2% saponin) for 1 hour prior to staining overnight with primary antibody diluted in blocking buffer. Anti-CD8 antibody (clone H35-17.2, BD bioscience)

was used at a dilution of 1:100 and anti-GFP antibody (Novus Biologicals, NB600-308) was used at 1:500 dilution to mark IFNγ from GREAT reporter mice. Slides were then washed three times with blocking buffer for 5 minutes prior to placing in secondary antibody diluted 1:1000 in blocking buffer. Finally, samples were mounted in Fluoroshield with DAPI (Sigma, F6057).

Images were recorded using a fluorescence microscope (Leica DM4B) with attached CCD microscope camera (Leica DFC3000g) at 400x total magnification. Eight unique fields of view were recorded for each slide resulting in a total of 24 fields of view collected for each tissue. Image quantification was performed using FIJI [79, 80]. For each image, the region of interest was manually drawn to capture the inflammatory infiltrate observed in between the epidermis and hypodermis. For each individual color channel, the smoothing function “Gaussian Blur” (settings: sigma = 0.2) was applied to reduce noise, a threshold was set manually to maximize the signal to noise ratio in the region of interest, and the FIJI particle analyzer (settings: size = 20-500; circularity = 0.3 – 1.00) was used to count the number of DAPI+ and CD8+ cells. For CD8+ cells, average pixel intensity for the IFNγ channel was also recorded, and if the intensity was greater than 20% of the maximum possible pixel intensity it was considered IFNγ+.

Cytokine measurements and detection

Cytokines were detected by ELISA, Luminex, western blot, or total protein as indicated. Luminex platform based assay for detection of multiple cytokines from Millipore was used to screen *L. major*. The following cytokines and chemokines were included: eotaxin, MCP-1, MCP-3, MIP-1α, MIP-1β, RANTES, Fractalkine, IL8, IL10, IL12p40, IL12p17, IL13, IL17A, IL1RA, IL1α, IL4, IL6, *7,* EGF, FGF2, FLT-3L, G-CSF, GM-CSF, PDGF-AA,

PDGF-BB, VEGF, IFNα2, IFNγ, TNFα, TNFβ, sCD40L, IL15, IL1β, IL2, IL3, IL5, IL8, TGFα, and MDC (Millipore). Cytokines below or above the limit of detection were excluded from analyses.

To interrogate the effect of GP63 on individual substrates, the following recombinant chemokines were used: human CXCL10 (R&D, 266-IP), mouse CXCL10 (R&D, 466-CR), human CXCL11 (R&D, 672-IT), human CXCL9 (Peprotech, 300-26), human CXCL8 (Peprotech, 200-08A), and human CCL22 (Peprotech, 300-36A). To separate chemokines based on size, all chemokines except for CXCL9 (which antibody required non-reducing conditions) were incubated at 97°C for 10 minutes in SDS-loading buffer in the presence of βME prior to loading in a 4-20% bis-tris polyacrylamide gels and running at 120V for 1 hour. For total protein, the Colloidal Blue Staining kit (Thermo Scientific, LC6025) was used per manufacturer's protocol. For western blotting, protein was transferred to a PVDF membrane using a Hoefer TE77X semi-dry transfer system. LiCor Odyssey (TBS) Blocking Buffer (VWR, 102971-244) was used to block for 1 hour at room temperature. The following primary antibodies were used to detect chemokines: human CXCL9 (R&D, MAB392-SP), human CXCL11 (MAB672-SP), human CXCL8 (Novus, MAB208-SP), human CCL22 (Novus, MAB336-SP). Primary antibodies were detected with IRDye secondary antibodies (Li-Cor) and developed using a LiCor Odyssey Infrared Imaging System (Li-Cor, 9120). Relative protein quantification based on band intensity was performed using the FIJI gel analysis function [79].

Expression of recombinant GP63 and site directed mutagenesis

Expression of CXCL10 and GP63 were performed by transfection in HEK293T cells. HEK293Ts were maintained in complete DMEM media supplemented with 10% FBS. Two days prior to transfection, 250,000 cells were washed and plated in a 6-well tissue culture treated plate in 2mL of serum free, FreeStyle 293 Expression Media (ThermoFisher, 12338018). One hour prior to transfection, media was replaced with fresh FreeStyle media. Transfection was performed with 2.5 total ng of endotoxin free plasmid DNA using the Lipofectamine 3000 Transfection Reagent Kit per manufacturer's instructions. Transfected HEK293Ts were incubated at 37°C for 48 hours prior to harvesting culture supernatant and storing in polypropylene, low-binding tubes (Corning, 29442-578) at -80°C until use.

The CXCL10 plasmid was obtained from Origene (NM_001565), and contains C-terminal Myc and Flag epitope tags. For GP63, a codon optimized plasmid was obtained from OriGene on the pcDNA3.1/Hygro plasmid backbone. Following a kozak sequence and secrecon to enhance secretion [81-83], GP63-1 based on the *L. major* Fd sequence (Q4QHH2-1) was inserted with the *Leishmania* specific secretion signal and GPI anchor motif removed (V100-N577) [84], and epitope tagged with Myc and His sequences placed at the C-terminus. Point mutations in CXCL10 and GP63 were made using the Agilent QuikChange Site Directed Mutagenesis kit according to manufacturer's instructions.

Mass spectrometry

CXCL10 exposed to GP63 for 5 hours, along with a negative (untreated) control was delivered in PAGE loading buffer at an approximate concentration of 30 ng/uL. Mass spectrometry was carried out by the Duke Proteomics and Metabolomics Shared

Resource. Molecular weight analysis of intact and cleaved CXCL10 from gel loading buffer was performed using a ZipChip CE system (908 Devices, Inc) coupled to a Q Exactive HF Orbitrap mass spectrometer (Thermo Scientific). Ammonium acetate was added to the sample to a final concentration 0.1 M, and 5µL of the loading buffer was pipetted manually into a HR ZipChip. Capillary electrophoresis (CE) separation was performed at 500 V/cm with a 30 second injection in Metabolite BGE (908 Devices, Inc). Mass spectrometry used positive electrospray with 120,000 Rs scan, 500-2000 m/z, 3e6 AGC target and 100 msec max ion injection time. Mass deconvolution was performed in Proteome Discoverer 2.2.

Tandem mass spectrometric sequencing of the cleaved and uncleaved fragments of CXCL10 after GP63 treatment, as well as an untreated control sample, were performed after gel separation on a 4-12% NuPAGE gel (Invitrogen). Gel bands were isolated after colloidal Coomassie staining, destained in acetonitrile/water, reduced with 10 mM DTT, alkylated with 20 mM iodoacetamide, and digested overnight at 37°C with 300 ng sequencing grade trypsin (Promega) in 50 mM ammonium bicarbonate at pH 8. Peptides were extracted in 1% formic acid and dried on a speedvac, then resuspended in a total of 10 µL 97/2/1 v/v/v water/acetonitrile/TFA. 4 µL of each sample was injected for analysis by LC-MS/MS using a 90 minute, 5-30% MeCN LC gradient and a top 12 DDA MS/MS method with MS1 at 120k and MS2 at 15k resolution. The data files were searched on Mascot v 2.5 with the UniProt database (downloaded November 2017) and *Homo sapiens* taxonomy selected, semitryptic specificity, along with fixed modification carbamidomethyl (C) and variable modifications oxidated (M), and deamidated (NQ). The results of the database searches were compiled into Scaffold v4 for curation. Using the search results

as a spectral library, Skyline v4.1 was used to extract peak intensities for peptides which looked to be a part of the cleavage region (residues 74-91) or non-cleaved region (residues 48-68), in order to more definitively localize the specific cleavage location (Figure 2E). Intensity was expressed as the peak area normalized to the protein region from residues 29-52, in order to control for protein abundance differences between the samples. The Skyline file has been made publicly available at Panoramaweb.org (https://goo.gl/4xsLsF).

Statistical analysis

All statistical analysis was performed using GraphPad Prism. Unpaired Student's T-test, one-way ANOVA, and two-way ANOVA with Tukey's post-hoc test were used as appropriate where indicated. The number of biological replicates (N) are indicated in the figure legend for each experiment and defined as follows. For *in vitro* cell culture and protein assessment each well of cells or chemokine prior to experimental manipulation (such as infection with parasite or addition of chemokine and/or inhibitor) was treated as a unique biological replicate. For *in vivo* murine models, each individual mouse was treated as a unique biological replicate. When technical replicates, repeated use of the same biological sample in a readout assay, were used they are indicated in the figure legend text and averaged values were combined into the single biological replicate prior to calculating statistics.

Acknowledgments

ALA, MIA, ET, KDG, KJP, and DCK were supported by Duke Molecular Genetics & Microbiology startup funds, Duke University Whitehead Scholarship, Butler Pioneer

Award, and NIH U19AI084044. ET was supported by the Duke Summer Research Opportunity Program (SROP). JSS and SR were supported by NIH GM122798 and the Burroughs Wellcome Fund Career Award for Medical Scientists. RLR was supported by NIH AI119004. We thank Robyn Guo for assistance with immunoblotting and Sarah Rains for assistance with sample prep for CXCL10 cleavage site identification. We thank the Duke University School of Medicine for the use of the Proteomics and Metabolomics Shared Resource.

Author contributions

All authors critically reviewed the manuscript and contributed input to the final submission. ALA, DCK, and RLR wrote the manuscript. ALA, DCK, RLR, JSS, and SR contributed to strategy and project planning. ALA, MIA, ET, KDG, KJP, ABB, JSS, RLR, and DCK carried out experiments and analysis.

Competing Interests

The authors declare that no competing interests exist.

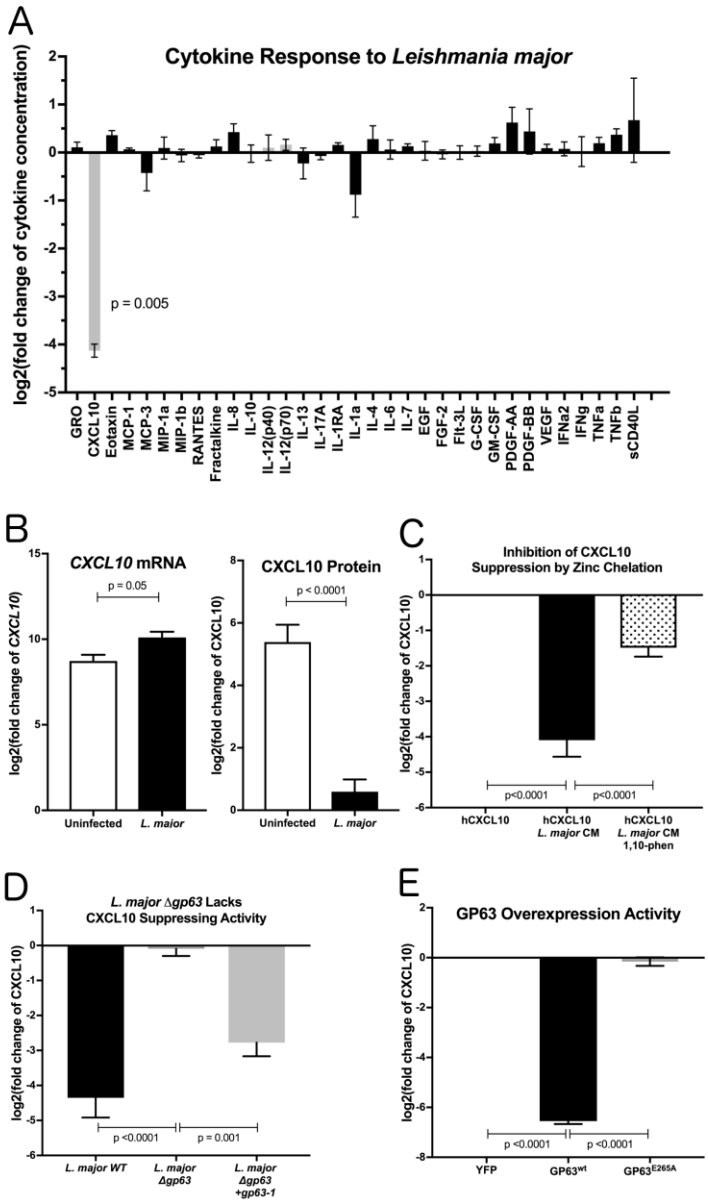

Figure 1. *Leishmania major* suppresses CXCL10 through proteolytic activity of glycoprotein-63. (A) Cytokine screening of LCLs exposed to *L. major* demonstrated suppression of CXCL10. Three lymphoblastoid cell lines (LCL), 7357, 18524, and 19203, were infected with *L. major.* Chemokines secreted into culture supernatants were analyzed by Luminex. Cytokines below the limit of detection were removed from the final analysis. Values are represented as $\log_2$ of the fold change relative to uninfected LCLs.

Type-1 associated cytokines are represented in grey. P-value represents Dunnett's post-hoc test compared to 1, after repeated measures one-way ANOVA. (B) CXCL10 produced by LPS stimulated THP-1 monocytes was suppressed by *L. major.* THP-1 monocytes were stimulated with LPS prior to *L. major* infection. CXCL10 mRNA was measured by qRT-PCR TaqMan assay using the $\Delta\Delta C_t$ method with 18s as housekeeping gene, and CXCL10 protein was measured by ELISA. For mRNA (n=3) and ELISA (n=6), Fold Change is relative to unstimulated, uninfected THP-1s. P-values calculated by student's T-test. (C) Zinc chelation prevents CXCL10 suppression. Concentration of human recombinant CXCL10 was measured by ELISA after incubation for 12 hours with filtered conditioned media from *L. major* WT promastigote culture and addition of the zinc-chelator 1,10-phenanthroline (n=8). (D) *gp63* is required for *L. major* CXCL10 suppression. Human recombinant CXCL10 concentrations were measured by ELISA after 12 hour incubation with conditioned media from *L. major* WT, Δ*gp63*, or Δ*gp63+1* (n=6). (E), GP63 expressed and secreted by HEK293Ts is sufficient for CXCL10 suppression. Human recombinant CXCL10 concentrations were measured by ELISA after 12 hour incubation with culture supernatant from HEK293Ts transfected with pCDNA3.1-gp63^{WT} or pCDNA3.1-gp63^{E285A} (n=7). For (C-E), P-values calculated by one-way ANOVA with Tukey's post-hoc test. Error bars represent standard error of the mean.

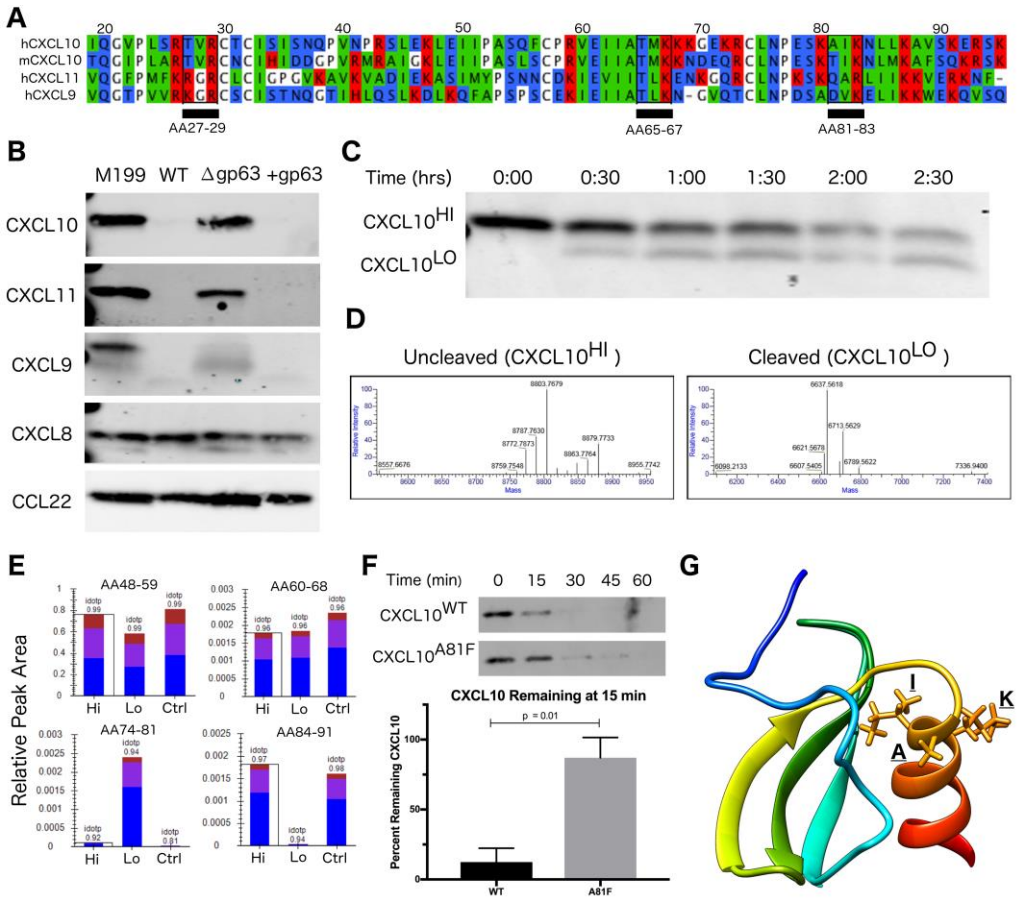

Figure 2. CXCL10 Cleavage by GP63 occurs between positions A81 and I82. (A) CXCL9/10/11 share significant homology at the amino-acid level. Multisequence alignment demonstrates that physical characteristics of amino acids are conserved across the CXCL10 family of chemokines. There are three putative GP63 cleavage sites (underlined) based on the consensus sequence of polar (P1), hydrophobic (P1'), basic (P2') [39]. (B) GP63 selectively cleaves chemokine ligands of the CXCR3 receptor. Conditioned media from *L. major WT, Δgp63,* and *Δgp63+1* was incubated with human recombinant chemokines for 12 hours and product detected by western blot. Cleavage is only detected for the CXCL9/10/11 family. (C) Cleavage by GP63 generates a smaller molecular weight protein. A time course of cleavage of human CXCL10 by heterologously expressed GP63 demonstrated an intermediate cleavage product, resolved by PAGE and Coomassie staining. (D) Cleavage by GP63 results in a change in CXCL10 molecular

weight of 2.2kD. Capillary electrophoresis-Mass Spectrometry (CE-MS) determined the molecular weight of the uncleaved ($CXCL10^{Hi}$) and cleaved ($CXCL10^{Lo}$) bands as 8.8kD and 6.6kD respectively. (E) Comparative analysis by trypsin digest of cleaved and uncleaved CXCL10 reveals cleavage occurring between A81-I82. Liquid chromatography-mass spectrometry (LC-MS) following trypsin digest of $CXCL10^{Hi}$ and $CXCL10^{Lo}$ identified peptide ending at A81, exclusively in the $CXCL10^{Lo}$ band, and a corresponding lack of peptide coverage from AA84-91. (F) Mutation of A81F significantly impairs GP63 cleavage of CXCL10. In the presence of GP63, $CXCL10^{A81F}$ remains stable for up to 45 minutes whereas $CXCL10^{WT}$ degradation is nearly complete by 15 minutes. Percentage of GP63 remaining at 15 minutes is plotted (n=3-4 per CXCL10 genotype). P-value calculated by Student's T-test. (G) The GP63 cleavage site is found on the C-terminal alpha-helix loop of CXCL10. Based on the NMR crystal structure of CXCL10 (Booth et al., 2002), the A81, I82, K83 (P1, P1', P2') GP63 cleavage motif maps to an exposed alpha-helical region.

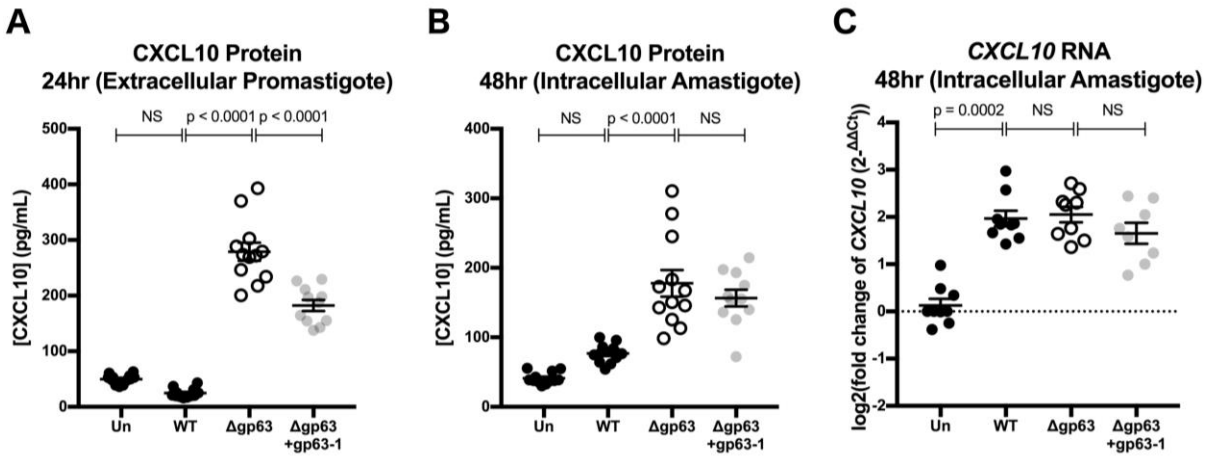

Figure 3. GP63 produced by *L. major* promastigotes and amastigotes cleaves CXCL10. (A) *L. major* promastigotes suppress CXCL10 through GP63 activity. THP-1 monocytes were differentiated using 100ng/mL of PMA prior to infection and CXCL10

concentration was assessed in the supernatant 24 hours post-infection by ELISA. (B) *L. major* amastigotes suppress CXCL10 through GP63 activity. At 24 hours post-infection, extracellular promastigotes were washed away from the differentiated THP-1 monocytes. At 48 hours post-infection the CXCL10 concentration was assessed in the supernatant by ELISA. For A-B, data represents four separate infections and was analyzed by one-way ANOVA with Tukey's post-hoc test (C) *L. major* induces similar levels of *CXCL10* mRNA, independent of GP63 genotype. At 48 hours post-infection, mRNA was extracted from PMA differentiated THP-1 monocytes and CXCL10 mRNA was measured by qRT-PCR TaqMan assay using the $\Delta\Delta C_t$ method with 18s as housekeeping gene. For C, data are from three separate experiments and were analyzed by one-way ANOVA with Tukey's post-hoc test.

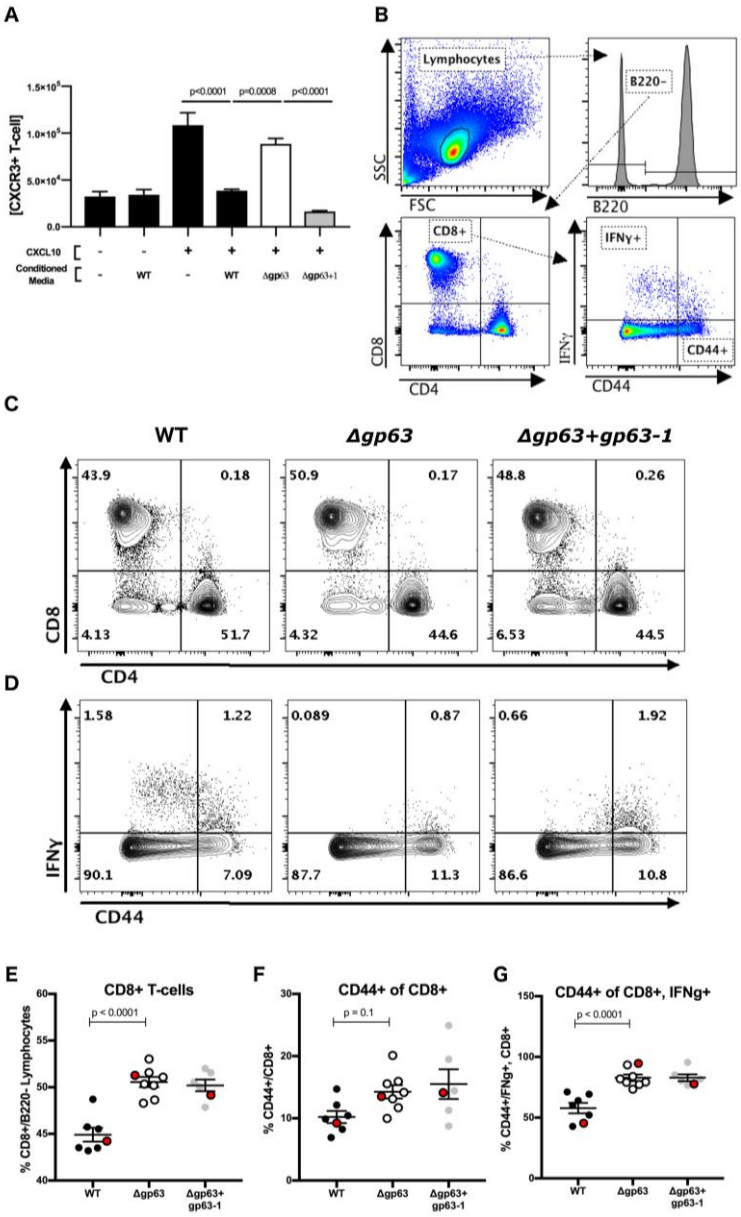

Figure 4. GP63 impairs CXCR3 mediated chemotaxis of activated CD8+ T cells. (A) CXCL10 incubated with GP63 is unable to chemoattract CXCR3+ cells *in vitro.* Jurkat T cells stably transfected with CXCR3 were seeded on the apical surface of a 5μm transwell insert, with human recombinant CXCL10 pre-incubated with conditioned media from either *L. major WT, Δgp63,* or *Δgp63+1* in the basal chamber. The number of CXCR3+ Jurkats in the basal chamber after 4 hours were counted to assess chemotactic capacity

of CXCL10 after exposure to GP63. (B-G) In C57BL/6J mice, *L. major Δgp63* infection alters CD8+ T cells in the draining lymph node. L*. major* WT*, Δgp63,* or *Δgp63+1* promastigotes were inoculated in the hind footpad of IFNγ reporter (GREAT) mice. Mice were infected in groups of 2-3 per parasite genotype over three separate sets of infections. To enable comparison across *L. major* genotypes, flow cytometry was performed on single cell suspensions from the draining lymph nodes at the earliest time point at which all genotypes elicited at least a 0.2mm change in footpad thickness (59 days post infection). (B) Gating strategy to identify changes in T cell subsets based on staining for B220, CD8, CD4, and CD44 in addition to the IFNγ-YFP reporter. (C) Representative plots demonstrating an increase in CD8+ T cells in *L. major Δgp63* infection. (D) Representative plots demonstrating an increase in CD44+ CD8+ T cells in *L. major Δgp63* infection. Representative samples displayed are indicated by red symbols in panels E-G. (E) The frequency of CD8+ T-cells is increased in *L. major Δgp63*-infected mice. Frequency of CD8+ cells was determined by first gating on live, singlet cells in the lymphocyte gate which stained B220- before separating based on CD4 and CD8 stain. (F) The frequency of CD8+ cells expressing CD44 is increased in *L. major Δgp63*-infected mice. CD8+ T cells were gated based on CD44 and IFNγ-YFP. Frequency of total CD44+ of CD8+ cells is plotted. (G) Within IFNγ+, CD8+ T cells, CD44 expression is further enriched. Data were normalized to the global mean, and P-values were generated by one-way ANOVA with Tukey's post-hoc test. Error bars represent standard error of the mean. ns, not significant.

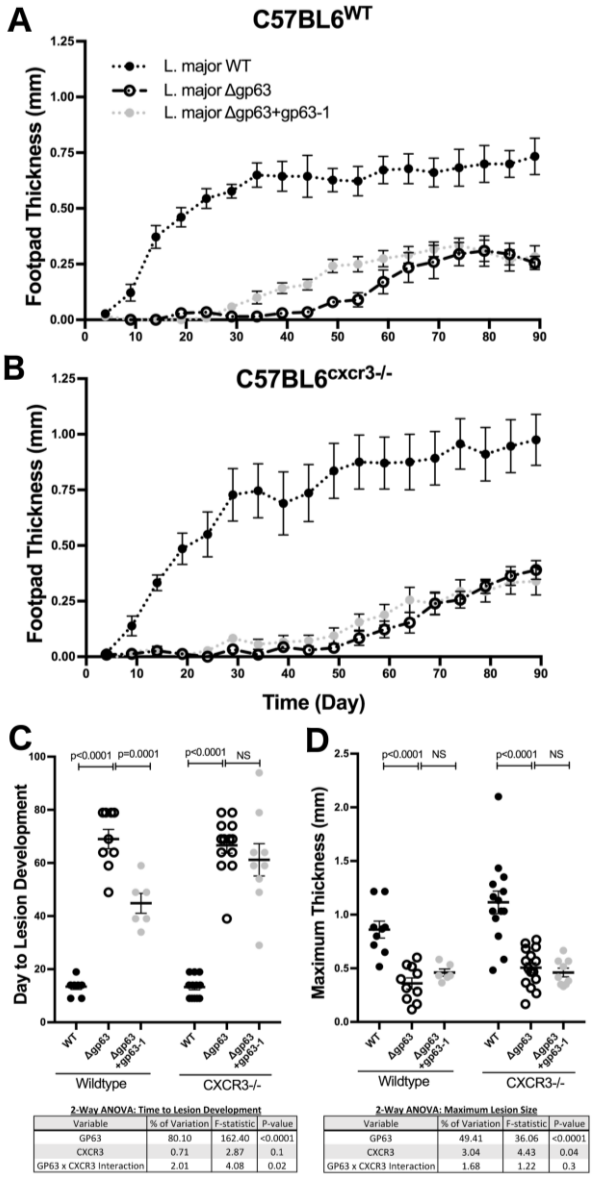

2-Way ANOVA: Time to Lesion Development

Variable	% of Variation	F-statistic	P-value
GP63	80.10	162.40	<0.0001
CXCR3	0.71	2.87	0.1
GP63 x CXCR3 Interaction	2.01	4.08	0.02

2-Way ANOVA: Maximum Lesion Size

Variable	% of Variation	F-statistic	P-value
GP63	49.41	36.06	<0.0001
CXCR3	3.04	4.43	0.04
GP63 x CXCR3 Interaction	1.68	1.22	0.3

Figure 5. Attenuated pathogenesis of *L. major Δgp63* in C57BL/6J mice partially depends on CXCR3 signaling. (A-B) *L. major Δgp63* impairs disease progression in C57BL/6J^{WT} relative to C57BL/6J$^{CXCR3-/-}$ mice. (A) C57BL/6J^{WT} mice were inoculated in the left hind footpad with 2X10^{6} promastigotes of either *L. major* WT (n=9), *Δgp63* (n=10), or *Δgp63+1* (n=6). All mice survived until the final experimental endpoint. (B) C57BL/6J$^{CXCR3-/-}$ mice were inoculated in the left hind footpad with 2X10^{6} promastigotes

of either *L. major* WT (n=14), *Δgp63* (n=15), or *Δgp63+1* (n=9). In the *L. major* WT group, two mice were sacrificed prior to the final experimental endpoint due to lesion ulceration qualifying as a humane endpoint. For A-B, Footpad thickness was monitored every 5 days for 4 months and is expressed relative to the contralateral, uninfected footpad. For each group, the mean difference in footpad thickness +/- the standard error of the mean is plotted over the first 90 days of infection. For the two mice sacrificed prior to the final experimental endpoint, the final measured lesion thickness was carried forward for future timepoints for calculating mean and standard error (C) *L. major Δgp63* delays the time to lesion development. *L. major Δgp63* infected mice develop lesions slower relative to *L. major Δgp63+1* in C57BL/6J^{WT} but not in C57BL/6J^{cxcr3}.The time to lesion onset was defined as the day a footpad demonstrated a relative increase of at least 0.2mm (D) GP63 and CXCR3 both impact maximum lesion size; however, *Cxcr3*$^{-/-}$ increases lesion size regardless of *gp63* genotype. Maximum thickness is defined as the average of the three highest measurements over the entire course of infection. For C-D, all individual mice are represented by symbols, with mean +/- standard error shown in bars, and P-values calculated by two-way ANOVA with Tukey's post-hoc test. Summary statistics from two-way ANOVA using *gp63* genotype and *Cxcr3* genotype as factors are displayed below the corresponding plot.

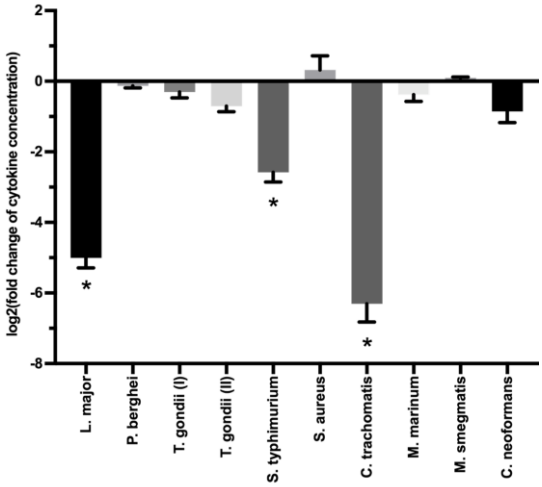

Figure 6. Multiple intracellular pathogens have evolved a mechanism for CXCL10 suppression. LCL 18524 was used to screen *L. major* (p=0.0001), *P. berghei* (p=0.99), *T. gondii* I (RH) (p=0.44), *T. gondii* II (Prugniaud A7) (p=0.011), *S. enterica* serovar Typhimurium (p=0.0001), *S. aureus* (p=0.12), *C. trachomatis* (p=0.0001), *M. marinum* (p=0.37), *M. smegmatis* (p>0.99), *and C. neoformans* (p=0.010) for CXCL10 suppressing activity (n=2-4 for each pathogen). CXCL10 was measured by ELISA and is represented as the $\log_2$ of fold change relative to uninfected controls. P-values calculated by one-way ANOVA with Dunnett's post-hoc test compared to a value of 1, which would represent no change. (*) represents p<0.01.

Supplemental Figures

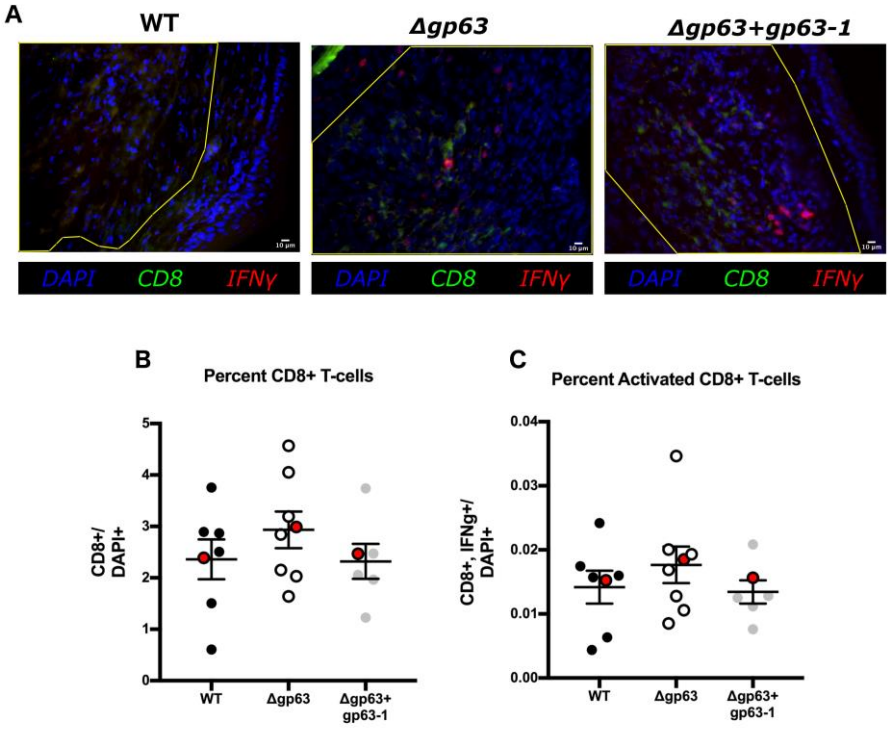

Figure S1. GP63 impairs chemotaxis of CD8+ T cells to the site of *L. major* infection. (A) Representative images of CD8+ cells at the site of the lesion in C57BL6^{GREAT} (IFNγ-YFP reporter) mice infected with *L. major* WT*, Δgp63,* or *Δgp63+1.* Representative images displayed are indicated by red symbols in B-C. (B) More CD8+ cells are found at the site of infection in *L. major Δgp63* infected mice compared to *L. major* WT. The difference is not statistically significant. (C) More IFNγ+ CD8+ cells are found at the site of infection in *L. major Δgp63* infected mice compared to *L. major* WT. The difference is not statistically significant. For B-C, data analyzed by one-way ANOVA with Tukey's post-hoc test.

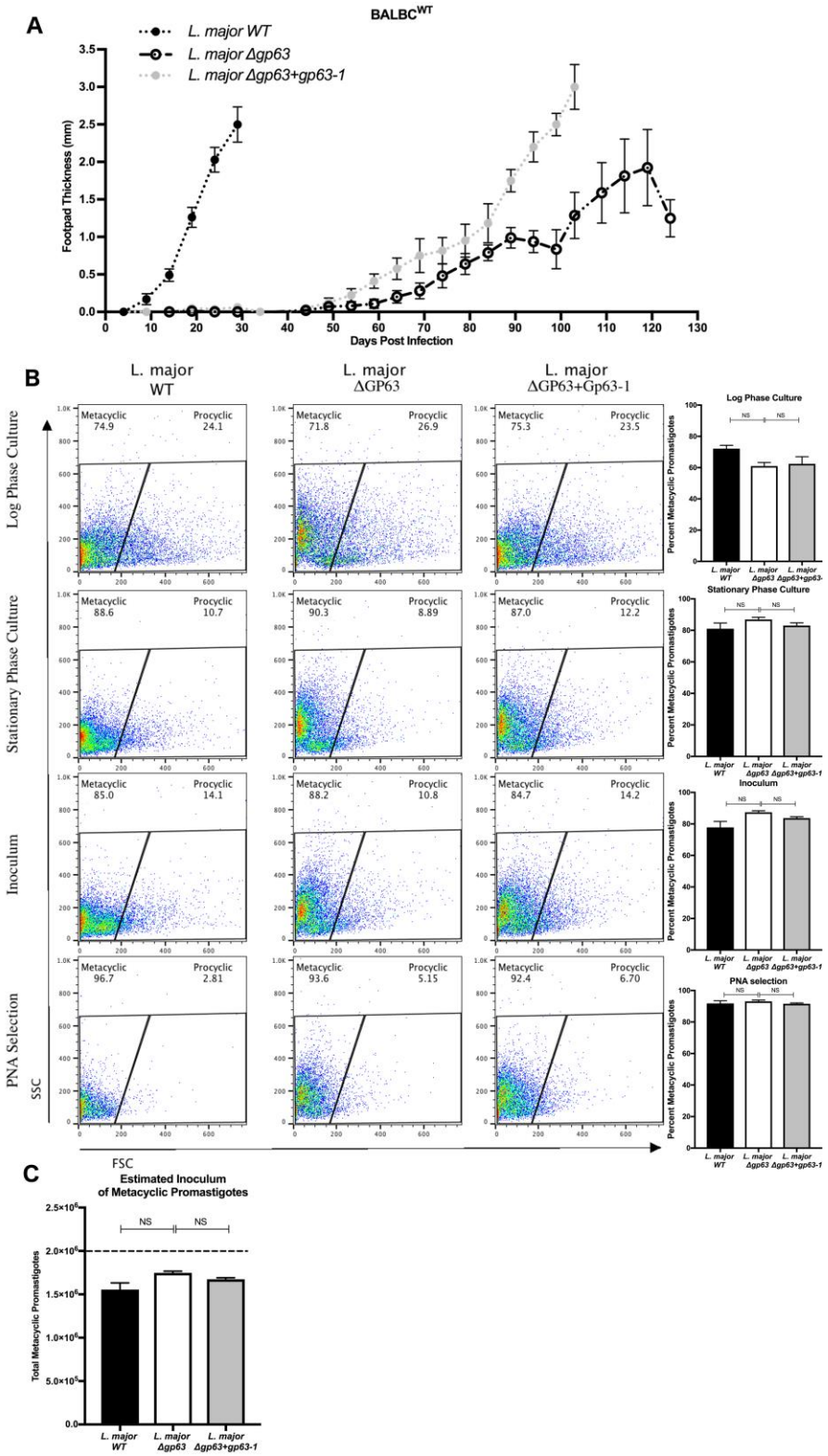

Figure S2. *Δgp63* impairs virulence of *L. major* in BALB/C mice, and *L. major* WT, *L. major Δgp63,* and *L. major Δgp63+1* undergo comparable rates of metacyclogenesis. (A)

Using the inoculum of total promastigotes resulted in infections consistent with the original report by Joshi et al., where deletion of GP63 (*Δgp63*) in *L. major* results in a delay in time to lesion development and maximum lesion size in BALB/c mice. Mice were inoculated in the left hind footpad with $2x10^6$ promastigotes of either *L. major* WT (n=5)*, Δgp63* (n=5)*,* or *Δgp63+1* (n=5)*.* Footpad thickness was monitored every 5 days for 4 months and is expressed relative to the contralateral, uninfected footpad. For each group, the mean footpad thickness +/- the standard error of the mean is plotted. (B) Flow cytometry and selection with peanut agglutinin (PNA) demonstrate that the three strains of *L. major* used in this study did not have significantly different rates of metacyclogenesis. Parasites were analyzed using a Guava EasyCyte-HT flow cytometer and gated based on forward scatter (FSC) and side scatter (SSC) as previously described [75]. Log-phase parasites were obtained from day 3 of culture, stationary phase parasites from day 5 of culture, the inoculum from day 5 culture after preparing parasites for infection as described in methods, and PNA selected from the inoculum after PNA selection. PNA selection was performed by incubating $1x10^8$ parasites in 100μg/mL of PNA (Vector Labs, L-1070-5) for 30 minutes at room temperature, followed by spinning for 5 minutes at 200xg, and taking the PNA- parasites in the supernatant for analysis. The PNA- parasites were then used as a control to define the gate for metacyclic promastigotes based on FSC and SSC. Conditions (n = 3 per group) were analyzed by one-way ANOVA with Tukeys post-hoc test. Not significant (NS) indicated $p > 0.05$. (C) There is no significant difference in estimated proportion of metacyclic promastigotes between *L. major* WT*, L. major Δgp63,* and *L. major Δgp63+1.* Estimated inoculum of metacyclic promastigotes was calculated

by multiplying the proportion of metacyclic promastigotes in the inoculum, as measured in A and B, by the total number of promastigotes used for infection: $2x10^6$.

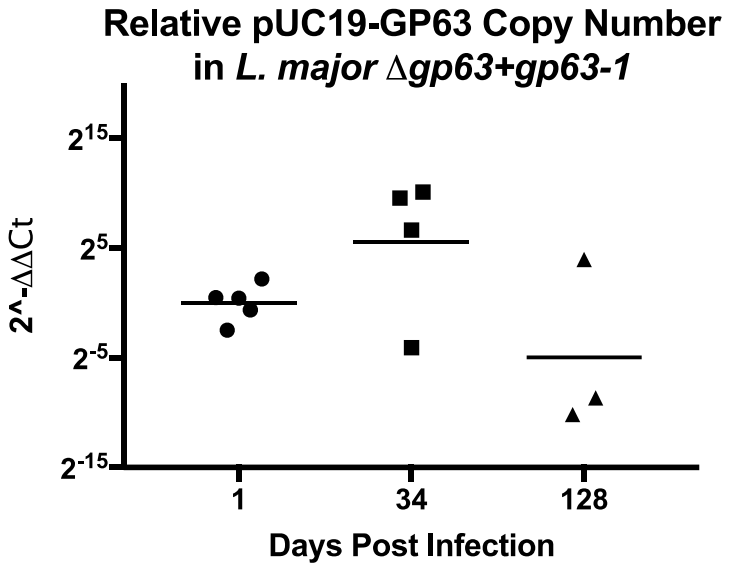

Figure S3. pUC19-GP63 is lost over the course of 128 day infections. Relative copy number of pUC19-GP63 was calculated by quantitative real-time PCR (qRT-PCR). A common region pUC19 of the pUC19 backbone was amplified as described previously [85] to obtain a pUC19-Ct value for each sample. Subsequently, each sample was normalized to the parasite burden (fg) as quantified by amplification of the DRBD3 gene and standardized by a standard curve of known parasite DNA. In order to enable analysis by the ΔΔCt method, the parasite burden (fg) was log_2 transformed. Relative copy number was then calculated as follows: $\Delta\mathrm{Ct} = Ct_{pUC19} - log_2(Parasite\ Burden\ (fg))$, $\Delta\Delta Ct = \Delta Ct_{Sample} - \Delta Ct_{1\ dpi}$. Fold change is shown as $2^{-\Delta\Delta\mathrm{Ct}}$, and the geometric mean for each time point is represented by a single line.

1. Reiner SL, Locksley RM. The regulation of immunity to Leishmania major. Annual review of immunology. 1995;13:151-77. doi: 10.1146/annurev.iy.13.040195.001055. PubMed PMID: 7612219.
2. Alvar J, Velez ID, Bern C, Herrero M, Desjeux P, Cano J, et al. Leishmaniasis worldwide and global estimates of its incidence. PLoS One. 2012;7(5):e35671. doi: 10.1371/journal.pone.0035671. PubMed PMID: 22693548; PubMed Central PMCID: PMCPMC3365071.
3. Okwor I, Uzonna JE. Immunotherapy as a strategy for treatment of leishmaniasis: a review of the literature. Immunotherapy. 2009;1(5):765-76. doi: 10.2217/imt.09.40. PubMed PMID: 20636022.
4. Scott P, Novais FO. Cutaneous leishmaniasis: immune responses in protection and pathogenesis. Nature reviews Immunology. 2016;16(9):581-92. doi: 10.1038/nri.2016.72. PubMed PMID: 27424773.
5. Reiner SL, Locksley RM. Cytokines in the differentiation of Th1/Th2 CD4+ subsets in leishmaniasis. J Cell Biochem. 1993;53(4):323-8. doi: 10.1002/jcb.240530409. PubMed PMID: 7905485.
6. Heinzel FP, Sadick MD, Holaday BJ, Coffman RL, Locksley RM. Reciprocal expression of interferon gamma or interleukin 4 during the resolution or progression of murine leishmaniasis. Evidence for expansion of distinct helper T cell subsets. J Exp Med. 1989;169(1):59-72. PubMed PMID: 2521244; PubMed Central PMCID: PMCPMC2189187.
7. Scott P, Natovitz P, Coffman RL, Pearce E, Sher A. CD4+ T cell subsets in experimental cutaneous leishmaniasis. Memorias do Instituto Oswaldo Cruz. 1988;83 Suppl 1:256-9. PubMed PMID: 3267029.
8. Ritter U, Korner H. Divergent expression of inflammatory dermal chemokines in cutaneous leishmaniasis. Parasite Immunol. 2002;24(6):295-301. PubMed PMID: 12102714.
9. Ajdary S, Alimohammadian MH, Eslami MB, Kemp K, Kharazmi A. Comparison of the immune profile of nonhealing cutaneous Leishmaniasis patients with those with active lesions and those who have recovered from infection. Infect Immun. 2000;68(4):1760-4. PubMed PMID: 10722561; PubMed Central PMCID: PMCPMC97345.
10. Carvalho EM, Correia Filho D, Bacellar O, Almeida RP, Lessa H, Rocha H. Characterization of the immune response in subjects with self-healing cutaneous leishmaniasis. Am J Trop Med Hyg. 1995;53(3):273-7. PubMed PMID: 7573712.
11. Castellano LR, Filho DC, Argiro L, Dessein H, Prata A, Dessein A, et al. Th1/Th2 immune responses are associated with active cutaneous leishmaniasis and clinical cure is associated with strong interferon-gamma production. Hum Immunol. 2009;70(6):383-90. doi: 10.1016/j.humimm.2009.01.007. PubMed PMID: 19480861.
12. Novais FO, Scott P. CD8+ T cells in cutaneous leishmaniasis: the good, the bad, and the ugly. Semin Immunopathol. 2015;37(3):251-9. doi: 10.1007/s00281-015-0475-7. PubMed PMID: 25800274; PubMed Central PMCID: PMCPMC4439344.
13. Oghumu S, Dong R, Varikuti S, Shawler T, Kampfrath T, Terrazas CA, et al. Distinct populations of innate CD8+ T cells revealed in a CXCR3 reporter mouse. J Immunol. 2013;190(5):2229-40. doi: 10.4049/jimmunol.1201170. PubMed PMID: 23338236; PubMed Central PMCID: PMCPMC3683850.

14. Belkaid Y, Von Stebut E, Mendez S, Lira R, Caler E, Bertholet S, et al. CD8+ T cells are required for primary immunity in C57BL/6 mice following low-dose, intradermal challenge with Leishmania major. J Immunol. 2002;168(8):3992-4000. PubMed PMID: 11937556.
15. Uzonna JE, Joyce KL, Scott P. Low dose Leishmania major promotes a transient T helper cell type 2 response that is down-regulated by interferon gamma-producing CD8+ T cells. J Exp Med. 2004;199(11):1559-66. doi: 10.1084/jem.20040172. PubMed PMID: 15184505; PubMed Central PMCID: PMCPMC2211781.
16. Muller I, Kropf P, Louis JA, Milon G. Expansion of gamma interferon-producing CD8+ T cells following secondary infection of mice immune to Leishmania major. Infect Immun. 1994;62(6):2575-81. PubMed PMID: 8188380; PubMed Central PMCID: PMCPMC186547.
17. Muller I, Kropf P, Etges RJ, Louis JA. Gamma interferon response in secondary Leishmania major infection: role of CD8+ T cells. Infect Immun. 1993;61(9):3730-8. PubMed PMID: 8359894; PubMed Central PMCID: PMCPMC281071.
18. Colmenares M, Kima PE, Samoff E, Soong L, McMahon-Pratt D. Perforin and gamma interferon are critical CD8+ T-cell-mediated responses in vaccine-induced immunity against Leishmania amazonensis infection. Infect Immun. 2003;71(6):3172-82. PubMed PMID: 12761096; PubMed Central PMCID: PMCPMC155724.
19. Novais FO, Carvalho LP, Graff JW, Beiting DP, Ruthel G, Roos DS, et al. Cytotoxic T cells mediate pathology and metastasis in cutaneous leishmaniasis. PLoS Pathog. 2013;9(7):e1003504. Epub 2013/07/23. doi: 10.1371/journal.ppat.1003504. PubMed PMID: 23874205; PubMed Central PMCID: PMCPMC3715507.
20. Groom JR, Luster AD. CXCR3 ligands: redundant, collaborative and antagonistic functions. Immunol Cell Biol. 2011;89(2):207-15. doi: 10.1038/icb.2010.158. PubMed PMID: 21221121; PubMed Central PMCID: PMCPMC3863330.
21. Qin S, Rottman JB, Myers P, Kassam N, Weinblatt M, Loetscher M, et al. The chemokine receptors CXCR3 and CCR5 mark subsets of T cells associated with certain inflammatory reactions. The Journal of clinical investigation. 1998;101(4):746-54. doi: 10.1172/JCI1422. PubMed PMID: 9466968; PubMed Central PMCID: PMCPMC508621.
22. Thomas SY, Hou R, Boyson JE, Means TK, Hess C, Olson DP, et al. CD1d-restricted NKT cells express a chemokine receptor profile indicative of Th1-type inflammatory homing cells. J Immunol. 2003;171(5):2571-80. PubMed PMID: 12928408.
23. Cella M, Jarrossay D, Facchetti F, Alebardi O, Nakajima H, Lanzavecchia A, et al. Plasmacytoid monocytes migrate to inflamed lymph nodes and produce large amounts of type I interferon. Nature medicine. 1999;5(8):919-23. doi: 10.1038/11360. PubMed PMID: 10426316.
24. Nanki T, Takada K, Komano Y, Morio T, Kanegane H, Nakajima A, et al. Chemokine receptor expression and functional effects of chemokines on B cells: implication in the pathogenesis of rheumatoid arthritis. Arthritis Res Ther. 2009;11(5):R149. doi: 10.1186/ar2823. PubMed PMID: 19804625; PubMed Central PMCID: PMCPMC2787286.
25. Vargas-Inchaustegui DA, Hogg AE, Tulliano G, Llanos-Cuentas A, Arevalo J, Endsley JJ, et al. CXCL10 production by human monocytes in response to Leishmania

braziliensis infection. Infect Immun. 2010;78(1):301-8. doi: 10.1128/IAI.00959-09. PubMed PMID: 19901067; PubMed Central PMCID: PMCPMC2798186.
26. Antoniazi S, Price HP, Kropf P, Freudenberg MA, Galanos C, Smith DF, et al. Chemokine gene expression in toll-like receptor-competent and -deficient mice infected with Leishmania major. Infect Immun. 2004;72(9):5168-74. doi: 10.1128/IAI.72.9.5168-5174.2004. PubMed PMID: 15322011; PubMed Central PMCID: PMCPMC517484.
27. Zaph C, Scott P. Interleukin-12 regulates chemokine gene expression during the early immune response to Leishmania major. Infect Immun. 2003;71(3):1587-9. PubMed PMID: 12595483; PubMed Central PMCID: PMCPMC148858.
28. Barbi J, Oghumu S, Rosas LE, Carlson T, Lu B, Gerard C, et al. Lack of CXCR3 delays the development of hepatic inflammation but does not impair resistance to Leishmania donovani. The Journal of infectious diseases. 2007;195(11):1713-7. doi: 10.1086/516787. PubMed PMID: 17471442.
29. Barbi J, Brombacher F, Satoskar AR. T cells from Leishmania major-susceptible BALB/c mice have a defect in efficiently up-regulating CXCR3 upon activation. J Immunol. 2008;181(7):4613-20. PubMed PMID: 18802063; PubMed Central PMCID: PMCPMC2562238.
30. Vasquez RE, Soong L. CXCL10/gamma interferon-inducible protein 10-mediated protection against Leishmania amazonensis infection in mice. Infect Immun. 2006;74(12):6769-77. doi: 10.1128/IAI.01073-06. PubMed PMID: 16982826; PubMed Central PMCID: PMCPMC1698098.
31. Gupta G, Bhattacharjee S, Bhattacharyya S, Bhattacharya P, Adhikari A, Mukherjee A, et al. CXC chemokine-mediated protection against visceral leishmaniasis: involvement of the proinflammatory response. The Journal of infectious diseases. 2009;200(8):1300-10. doi: 10.1086/605895. PubMed PMID: 19743920.
32. Gupta G, Majumdar S, Adhikari A, Bhattacharya P, Mukherjee AK, Majumdar SB, et al. Treatment with IP-10 induces host-protective immune response by regulating the T regulatory cell functioning in Leishmania donovani-infected mice. Med Microbiol Immunol. 2011;200(4):241-53. doi: 10.1007/s00430-011-0197-y. PubMed PMID: 21533785.
33. Vester B, Muller K, Solbach W, Laskay T. Early gene expression of NK cell-activating chemokines in mice resistant to Leishmania major. Infect Immun. 1999;67(6):3155-9. PubMed PMID: 10338536; PubMed Central PMCID: PMC96637.
34. Valdivia HO, Scholte LL, Oliveira G, Gabaldon T, Bartholomeu DC. The Leishmania metaphylome: a comprehensive survey of Leishmania protein phylogenetic relationships. BMC Genomics. 2015;16:887. doi: 10.1186/s12864-015-2091-2. PubMed PMID: 26518129; PubMed Central PMCID: PMC4628237.
35. Olivier M, Atayde VD, Isnard A, Hassani K, Shio MT. Leishmania virulence factors: focus on the metalloprotease GP63. Microbes Infect. 2012;14(15):1377-89. doi: 10.1016/j.micinf.2012.05.014. PubMed PMID: 22683718.
36. Voth BR, Kelly BL, Joshi PB, Ivens AC, McMaster WR. Differentially expressed Leishmania major gp63 genes encode cell surface leishmanolysin with distinct signals for glycosylphosphatidylinositol attachment. Molecular and biochemical parasitology. 1998;93(1):31-41. PubMed PMID: 9662026.
37. Fernandes MC, Dillon LA, Belew AT, Bravo HC, Mosser DM, El-Sayed NM. Dual Transcriptome Profiling of Leishmania-Infected Human Macrophages Reveals Distinct

Reprogramming Signatures. MBio. 2016;7(3). doi: 10.1128/mBio.00027-16. PubMed PMID: 27165796; PubMed Central PMCID: PMCPMC4959658.
38. Chaudhuri G, Chaudhuri M, Pan A, Chang KP. Surface acid proteinase (gp63) of Leishmania mexicana. A metalloenzyme capable of protecting liposome-encapsulated proteins from phagolysosomal degradation by macrophages. J Biol Chem. 1989;264(13):7483-9. PubMed PMID: 2708373.
39. Bouvier J, Schneider P, Etges R, Bordier C. Peptide substrate specificity of the membrane-bound metalloprotease of Leishmania. Biochemistry. 1990;29(43):10113-9. PubMed PMID: 2271643.
40. Booth V, Keizer DW, Kamphuis MB, Clark-Lewis I, Sykes BD. The CXCR3 binding chemokine IP-10/CXCL10: structure and receptor interactions. Biochemistry. 2002;41(33):10418-25. PubMed PMID: 12173928.
41. Joshi PB, Sacks DL, Modi G, McMaster WR. Targeted gene deletion of Leishmania major genes encoding developmental stage-specific leishmanolysin (GP63). Molecular microbiology. 1998;27(3):519-30. PubMed PMID: 9489664.
42. Reinhardt RL, Liang HE, Locksley RM. Cytokine-secreting follicular T cells shape the antibody repertoire. Nat Immunol. 2009;10(4):385-93. doi: 10.1038/ni.1715. PubMed PMID: 19252490; PubMed Central PMCID: PMC2714053.
43. Reinhardt RL, Liang HE, Bao K, Price AE, Mohrs M, Kelly BL, et al. A novel model for IFN-gamma-mediated autoinflammatory syndromes. J Immunol. 2015;194(5):2358-68. doi: 10.4049/jimmunol.1401992. PubMed PMID: 25637019; PubMed Central PMCID: PMC4337485.
44. Ogasawara W, Kobayashi G, Ishimaru S, Okada H, Morikawa Y. The gene encoding dipeptidyl aminopeptidase BI from Pseudomonas sp. WO24: cloning, sequencing and expression in Escherichia coli. Gene. 1998;206(2):229-36. Epub 1998/04/04. PubMed PMID: 9469937.
45. Joshi PB, Kelly BL, Kamhawi S, Sacks DL, McMaster WR. Targeted gene deletion in Leishmania major identifies leishmanolysin (GP63) as a virulence factor. Mol Biochem Parasitol. 2002;120(1):33-40. PubMed PMID: 11849703.
46. Anderson CF, Mendez S, Sacks DL. Nonhealing infection despite Th1 polarization produced by a strain of Leishmania major in C57BL/6 mice. J Immunol. 2005;174(5):2934-41. PubMed PMID: 15728505.
47. Rosas LE, Barbi J, Lu B, Fujiwara Y, Gerard C, Sanders VM, et al. CXCR3-/- mice mount an efficient Th1 response but fail to control Leishmania major infection. Eur J Immunol. 2005;35(2):515-23. doi: 10.1002/eji.200425422. PubMed PMID: 15668916.
48. Hu JK, Kagari T, Clingan JM, Matloubian M. Expression of chemokine receptor CXCR3 on T cells affects the balance between effector and memory CD8 T-cell generation. Proc Natl Acad Sci U S A. 2011;108(21):E118-27. doi: 10.1073/pnas.1101881108. PubMed PMID: 21518913; PubMed Central PMCID: PMCPMC3102421.
49. Harris TH, Banigan EJ, Christian DA, Konradt C, Wojno EDT, Norose K, et al. Generalized Levy walks and the role of chemokines in migration of effector CD8(+) T cells. Nature. 2012;486(7404):545-U145. doi: 10.1038/nature11098. PubMed PMID: WOS:000305760600046.
50. Majumder S, Bhattacharjee S, Paul Chowdhury B, Majumdar S. CXCL10 is critical for the generation of protective CD8 T cell response induced by antigen pulsed

CpG-ODN activated dendritic cells. PLoS One. 2012;7(11):e48727. doi: 10.1371/journal.pone.0048727. PubMed PMID: 23144947; PubMed Central PMCID: PMCPMC3492407.
51. Bousoffara T, Louzir H, Ben Salah A, Dellagi K. Analysis of granzyme B activity as a surrogate marker of Leishmania-specific cell-mediated cytotoxicity in zoonotic cutaneous leishmaniasis. The Journal of infectious diseases. 2004;189(7):1265-73. doi: 10.1086/382031. PubMed PMID: 15031796.
52. da Conceicao-Silva F, Perlaza BL, Louis JA, Romero P. Leishmania major infection in mice primes for specific major histocompatibility complex class I-restricted CD8+ cytotoxic T cell responses. Eur J Immunol. 1994;24(11):2813-7. doi: 10.1002/eji.1830241135. PubMed PMID: 7957573.
53. Ivens AC, Peacock CS, Worthey EA, Murphy L, Aggarwal G, Berriman M, et al. The genome of the kinetoplastid parasite, Leishmania major. Science. 2005;309(5733):436-42. doi: 10.1126/science.1112680. PubMed PMID: 16020728; PubMed Central PMCID: PMC1470643.
54. Seyed N, Peters NC, Rafati S. Translating Observations From Leishmanization Into Non-Living Vaccines: The Potential of Dendritic Cell-Based Vaccination Strategies Against Leishmania. Front Immunol. 2018;9:1227. doi: 10.3389/fimmu.2018.01227. PubMed PMID: 29922288; PubMed Central PMCID: PMCPMC5996938.
55. Singh S. Changing trends in the epidemiology, clinical presentation, and diagnosis of Leishmania-HIV co-infection in India. Int J Infect Dis. 2014;29:103-12. doi: 10.1016/j.ijid.2014.07.011. PubMed PMID: 25449244.
56. Lindoso JA, Cota GF, da Cruz AM, Goto H, Maia-Elkhoury AN, Romero GA, et al. Visceral leishmaniasis and HIV coinfection in Latin America. PLoS Negl Trop Dis. 2014;8(9):e3136. doi: 10.1371/journal.pntd.0003136. PubMed PMID: 25233461; PubMed Central PMCID: PMCPMC4169383.
57. Monge-Maillo B, Norman FF, Cruz I, Alvar J, Lopez-Velez R. Visceral leishmaniasis and HIV coinfection in the Mediterranean region. PLoS Negl Trop Dis. 2014;8(8):e3021. doi: 10.1371/journal.pntd.0003021. PubMed PMID: 25144380; PubMed Central PMCID: PMCPMC4140663.
58. Romano A, Carneiro MBH, Doria NA, Roma EH, Ribeiro-Gomes FL, Inbar E, et al. Divergent roles for Ly6C+CCR2+CX3CR1+ inflammatory monocytes during primary or secondary infection of the skin with the intra-phagosomal pathogen Leishmania major. PLoS Pathog. 2017;13(6):e1006479. doi: 10.1371/journal.ppat.1006479. PubMed PMID: 28666021; PubMed Central PMCID: PMCPMC5509374.
59. Glennie ND, Scott P. Memory T cells in cutaneous leishmaniasis. Cellular immunology. 2016;309:50-4. doi: 10.1016/j.cellimm.2016.07.010. PubMed PMID: 27493096; PubMed Central PMCID: PMCPMC5127769.
60. Glennie ND, Yeramilli VA, Beiting DP, Volk SW, Weaver CT, Scott P. Skin-resident memory CD4+ T cells enhance protection against Leishmania major infection. J Exp Med. 2015;212(9):1405-14. doi: 10.1084/jem.20142101. PubMed PMID: 26216123; PubMed Central PMCID: PMCPMC4548053.
61. Julia V, Glaichenhaus N. CD4(+) T cells which react to the Leishmania major LACK antigen rapidly secrete interleukin-4 and are detrimental to the host in resistant B10.D2 mice. Infect Immun. 1999;67(7):3641-4. PubMed PMID: 10377151; PubMed Central PMCID: PMCPMC116556.

62. Mazumder S, Maji M, Das A, Ali N. Potency, efficacy and durability of DNA/DNA, DNA/protein and protein/protein based vaccination using gp63 against Leishmania donovani in BALB/c mice. PLoS One. 2011;6(2):e14644. doi: 10.1371/journal.pone.0014644. PubMed PMID: 21311597; PubMed Central PMCID: PMCPMC3032732.
63. Mazumder S, Maji M, Ali N. Potentiating effects of MPL on DSPC bearing cationic liposomes promote recombinant GP63 vaccine efficacy: high immunogenicity and protection. PLoS Negl Trop Dis. 2011;5(12):e1429. doi: 10.1371/journal.pntd.0001429. PubMed PMID: 22206029; PubMed Central PMCID: PMCPMC3243702.
64. Bhowmick S, Ravindran R, Ali N. gp63 in stable cationic liposomes confers sustained vaccine immunity to susceptible BALB/c mice infected with Leishmania donovani. Infect Immun. 2008;76(3):1003-15. doi: 10.1128/IAI.00611-07. PubMed PMID: 18195029; PubMed Central PMCID: PMCPMC2258822.
65. Sachdeva R, Banerjea AC, Malla N, Dubey ML. Immunogenicity and efficacy of single antigen Gp63, polytope and polytopeHSP70 DNA vaccines against visceral Leishmaniasis in experimental mouse model. PLoS One. 2009;4(12):e7880. doi: 10.1371/journal.pone.0007880. PubMed PMID: 19956549; PubMed Central PMCID: PMCPMC2780826.
66. von Schillde MA, Hormannsperger G, Weiher M, Alpert CA, Hahne H, Bauerl C, et al. Lactocepin secreted by Lactobacillus exerts anti-inflammatory effects by selectively degrading proinflammatory chemokines. Cell Host Microbe. 2012;11(4):387-96. doi: 10.1016/j.chom.2012.02.006. PubMed PMID: 22520466.
67. Karlsson C, Eliasson M, Olin AI, Morgelin M, Karlsson A, Malmsten M, et al. SufA of the opportunistic pathogen finegoldia magna modulates actions of the antibacterial chemokine MIG/CXCL9, promoting bacterial survival during epithelial inflammation. J Biol Chem. 2009;284(43):29499-508. doi: 10.1074/jbc.M109.025957. PubMed PMID: 19628464; PubMed Central PMCID: PMCPMC2785583.
68. Jauregui CE, Wang Q, Wright CJ, Takeuchi H, Uriarte SM, Lamont RJ. Suppression of T-cell chemokines by Porphyromonas gingivalis. Infect Immun. 2013;81(7):2288-95. doi: 10.1128/IAI.00264-13. PubMed PMID: 23589576; PubMed Central PMCID: PMCPMC3697598.
69. Shiraki Y, Ishibashi Y, Hiruma M, Nishikawa A, Ikeda S. Candida albicans abrogates the expression of interferon-gamma-inducible protein-10 in human keratinocytes. FEMS Immunol Med Microbiol. 2008;54(1):122-8. doi: 10.1111/j.1574-695X.2008.00457.x. PubMed PMID: 18647352.
70. Casrouge A, Decalf J, Ahloulay M, Lababidi C, Mansour H, Vallet-Pichard A, et al. Evidence for an antagonist form of the chemokine CXCL10 in patients chronically infected with HCV. The Journal of clinical investigation. 2011;121(1):308-17. doi: 10.1172/JCI40594. PubMed PMID: 21183794; PubMed Central PMCID: PMCPMC3007131.
71. Harth-Hertle ML, Scholz BA, Erhard F, Glaser LV, Dolken L, Zimmer R, et al. Inactivation of intergenic enhancers by EBNA3A initiates and maintains polycomb signatures across a chromatin domain encoding CXCL10 and CXCL9. PLoS Pathog. 2013;9(9):e1003638. doi: 10.1371/journal.ppat.1003638. PubMed PMID: 24068939; PubMed Central PMCID: PMCPMC3777872.

72. Bowen JR, Quicke KM, Maddur MS, O'Neal JT, McDonald CE, Fedorova NB, et al. Zika Virus Antagonizes Type I Interferon Responses during Infection of Human Dendritic Cells. PLoS Pathog. 2017;13(2):e1006164. doi: 10.1371/journal.ppat.1006164. PubMed PMID: 28152048; PubMed Central PMCID: PMCPMC5289613.
73. Chaudhary V, Yuen KS, Chan JF, Chan CP, Wang PH, Cai JP, et al. Selective Activation of Type II Interferon Signaling by Zika Virus NS5 Protein. Journal of virology. 2017;91(14). doi: 10.1128/JVI.00163-17. PubMed PMID: 28468880; PubMed Central PMCID: PMCPMC5487581.
74. Consortium IH. A haplotype map of the human genome. Nature. 2005;437(7063):1299-320. Epub 2005/10/29. doi: 10.1038/nature04226. PubMed PMID: 16255080.
75. Saraiva EM, Pinto-da-Silva LH, Wanderley JL, Bonomo AC, Barcinski MA, Moreira ME. Flow cytometric assessment of Leishmania spp metacyclic differentiation: validation by morphological features and specific markers. Exp Parasitol. 2005;110(1):39-47. doi: 10.1016/j.exppara.2005.01.004. PubMed PMID: 15804377.
76. Sacks DL, Melby PC. Animal models for the analysis of immune responses to leishmaniasis. Curr Protoc Immunol. 2001;Chapter 19:Unit 19 2. doi: 10.1002/0471142735.im1902s28. PubMed PMID: 18432753; PubMed Central PMCID: PMCPMC4363783.
77. Antonia AL, Wang L, Ko DC. A real-time PCR assay for quantification of parasite burden in murine models of leishmaniasis. PeerJ. 2018;6:e5905. doi: 10.7717/peerj.5905. PubMed PMID: 30430041; PubMed Central PMCID: PMCPMC6231426.
78. Wang L, Pittman KJ, Barker JR, Salinas RE, Stanaway IB, Williams GD, et al. An Atlas of Genetic Variation Linking Pathogen-Induced Cellular Traits to Human Disease. Cell Host Microbe. 2018;24(2):308-23 e6. Epub 2018/08/10. doi: 10.1016/j.chom.2018.07.007. PubMed PMID: 30092202; PubMed Central PMCID: PMCPMC6093297.
79. Schindelin J, Arganda-Carreras I, Frise E, Kaynig V, Longair M, Pietzsch T, et al. Fiji: an open-source platform for biological-image analysis. Nature methods. 2012;9(7):676-82. doi: 10.1038/nmeth.2019. PubMed PMID: 22743772; PubMed Central PMCID: PMCPMC3855844.
80. Schneider CA, Rasband WS, Eliceiri KW. NIH Image to ImageJ: 25 years of image analysis. Nature methods. 2012;9(7):671-5. PubMed PMID: 22930834; PubMed Central PMCID: PMCPMC5554542.
81. Kozak M. The scanning model for translation: an update. J Cell Biol. 1989;108(2):229-41. PubMed PMID: 2645293; PubMed Central PMCID: PMCPMC2115416.
82. Barash S, Wang W, Shi Y. Human secretory signal peptide description by hidden Markov model and generation of a strong artificial signal peptide for secreted protein expression. Biochemical and biophysical research communications. 2002;294(4):835-42. doi: 10.1016/S0006-291X(02)00566-1. PubMed PMID: 12061783.
83. Guler-Gane G, Kidd S, Sridharan S, Vaughan TJ, Wilkinson TC, Tigue NJ. Overcoming the Refractory Expression of Secreted Recombinant Proteins in Mammalian Cells through Modification of the Signal Peptide and Adjacent Amino Acids.

PLoS One. 2016;11(5):e0155340. doi: 10.1371/journal.pone.0155340. PubMed PMID: 27195765; PubMed Central PMCID: PMCPMC4873207.

84. Schlagenhauf E, Etges R, Metcalf P. The crystal structure of the Leishmania major surface proteinase leishmanolysin (gp63). Structure. 1998;6(8):1035-46. PubMed PMID: 9739094.

85. Zhang Q, Wang J, Deng F, Yan Z, Xia Y, Wang Z, et al. TqPCR: A Touchdown qPCR Assay with Significantly Improved Detection Sensitivity and Amplification Efficiency of SYBR Green qPCR. PLoS One. 2015;10(7):e0132666. doi: 10.1371/journal.pone.0132666. PubMed PMID: 26172450; PubMed Central PMCID: PMCPMC4501803.